

Survey of very broad Diffuse Interstellar Bands

G. Galazutdinov

Instituto de Astronomia, Universidad Catolica del Norte, Av. Angamos 0610, Antofagasta,
Chile

Pulkovo Observatory, Pulkovskoe Shosse 65, Saint-Petersburg 196140, Russia

runizag@gmail.com

A. Bondar

ICAMER Observatory, NAS of Ukraine, Acad. Zabolotnoho 27, 03143, Kyiv, Ukraine

arctur.ab@gmail.com

Byeong-Cheol Lee

Korea Astronomy and Space Science Institute, 776, Daedeokdae-ro, Yuseong-gu, Daejeon,
Korea 34055

bcllee@kasi.re.kr

R. Hakalla, W. Szajna and J. Krełowski

Institute of Physics, University of Rzeszów, Pigonia 1 Street, 35-310, Rzeszów, Poland

hakalla@ur.edu.pl; szajna@ur.edu.pl; jacek@umk.pl

Received _____; accepted _____

ABSTRACT

This paper considers a very special set of a few interstellar features — broad diffuse interstellar bands (DIBs) at 4430, 4882, 5450, 5779 and 6175 Å. The set is small, and measurements of equivalent widths of these DIBs are challenging because of severe stellar, interstellar, and sometimes, also telluric contaminations inside their broad profiles. Nevertheless, we demonstrate that they do correlate pretty tightly (DIBs 4882 and 5450 to a lesser extent though) with other narrower diffuse bands, as well as with the color excess $E(B-V)$. The studied broad DIBs correlate well with both interstellar molecule CH and interstellar KI, i.e. it is hardly possible to verify whether the environments, facilitating the formation of very broad DIB carriers, are dominated by either molecular or atomic gas as both these species likely occupy the same volume.

Subject headings: ISM: clouds — ISM: lines and bands — ISM: molecules — ISM: individual objects (very broad DIBs)

1. Introduction

The diffuse interstellar bands (DIBs) have been known since nearly 100 yr (Heger 1922) but still remain unidentified. For a recent review see Krełowski (2018). The recently promoted identification of a few near infrared DIBs as being carried by C_{60}^+ (Cordiner, Linnartz, Cox et al. (2019) and references therein) does not take into account the fact that the two strongest DIBs do not show the laboratory predicted strength ratio and thus those of weaker bands are very uncertain (Galazutdinov et al. (2017), Galazutdinov & Krełowski (2017)). DIB profiles are always broader than those of interstellar atomic lines or those of simple interstellar radicals (CH , CN , CH^+). The most recent survey of DIBs (Fan et al., 2019) reports the presence of 556 features in the optical range. However, several DIBs have been discovered also in the infrared part of spectrum, see e.g. Galazutdinov et al. (2017) and references therein. In turn, diffuse bands are tentatively divided into two or three non-equal groups: the first group is the most numerous one of so-called narrow diffuse bands with a typical full width at the half maximum (FWHM) close to $\sim 1 \text{ \AA}$ the second contains a few features with $\text{FWHM} \sim 4 \text{ \AA}$, and the third one is a small group of broad DIBs with $\text{FWHM} \geq 10 \text{ \AA}$. In the current research we focus on it. Let us emphasize that the difference between broad and narrow diffuse bands is of physical origin. Perhaps, they are formed by different kinds of molecules. Indeed, the broad DIBs are well seen in targets being in the environment characterized by strong UV flux, e.g. in σ type objects, where for so-called narrow DIBs, the features that seem to be related to absorption features of simple interstellar radicals (CH , CN , CH^+) are very weak (see Krełowski (2018) and references therein).

The first very broad DIB, centered at $\sim 4430 \text{ \AA}$ was identified as such more than 80 yr ago (Beals & Blanchet (1938); Merrill & Humason (1938)). The band, as broad as about 40 \AA , $\text{FWHM} \sim 20 \text{ \AA}$ was found as stationary in a spectroscopic binary. It was reasonably

easy to demonstrate that the strength of this feature correlates with a color excess but precise measurements were difficult since the very broad profile was naturally contaminated (especially in B-type stars) with numerous stellar lines of various intensity (Herbig 1966). This is why the first determined correlations between 4430 and color excess or intensities of other interstellar features were found to be reasonably poor (Greenstein & Aller 1950).

The discovered later, 6170 DIB, is the only very broad DIB that is not severely contaminated with stellar lines (Rudkjøbing 1970). The latter publication reported the 4430/6175 strength ratio to be related to the galactic longitude and to the total-to-selective extinction ratio. The conclusion was, however, based on a rather small sample of reddened stars. We found that the 6170 diffuse band is often blended with another broad DIB marked as 6177 Å one. Also, this double-DIB is often blended with many narrow diffuse bands (Galazutdinov et al., 2000, Hobbs et al., 2008), challenging the measurements. Here we measured the features of 6170 and 6177 together and marked the resulting one as 6175 DIB.

Diffuse bands' intensities, especially of 4430, have been typically related to the continuous extinction curve (Herbig 1967). Until the end of the 1960s the 4430 DIB was the most frequently investigated diffuse feature. The band is the first DIB observed outside our Milky Way system (Houziaux, Nandy & Morgan 1980). Until the beginning of the 1980s the hypothesis that the DIBs are carried by dust grains was taken very seriously. Herbig (1967) compared the problem of DIB identification to those of nebulium and coronium, saying that its solution may be of similar importance.

A statistical investigation of 65 sources revealed a rather tight correlation between the color excess and the 4430 DIB intensity (Gammelgaard 1975). The relation suffers, however, a rather serious scatter among heavily reddened targets. Soon after the extra-atmospheric observations have been launched, Danks (1980) suggested the correlation between the 4430 DIB and the 2200 bump of the extinction curve. Isobe et al. (1986) analyzed a sample of

482 reddened stars. Their 4430 strengths do correlate with E(B–V) but the scatter is very substantial.

A real breakthrough in the DIB investigations was the publication of Herbig (1975) which, due to the enhanced signal-to-noise (S/N) ratio, raised the number of known DIBs from 9 to 39 features plus a few suspects. Herbig demonstrated quite narrow DIBs (like 6196 or 6379), as well as pretty broad (like 5780 or 6284) and very broad ones (like 4882 or 6175). All these features' intensities showed a rather tight correlations with the E(B–V). The Herbig's investigation was based on averaged spectra with S/N~100. A statistically valuable sample of the 4430 central depth in low-resolution, high-S/N spectra (Krełowski et al. 1987) suggested the local differences in relative strengths of the very broad feature. The paper emphasized the problem of the profile stellar contaminations. Later the very broad DIBs were investigated rather seldomly.

The recent paper of (Sonnenrecker et al. 2018) revitalized the idea of investigating the broadest diffuse bands. They studied 21 sightlines and demonstrated profiles of a few broad DIBs, but only the relation of 6175 to E(B–V). Moreover, they analyzed correlations between the broad DIBs and narrower ones. In their opinion the 4963 DIB originates in rather molecular gas while 5780, 5797, 6284, and 6613 Å DIBs primarily trace atomic gas. Our idea is to check the above-mentioned suggestions using a larger sample of much higher resolution spectra.

2. Observational data

Our observations have been collected using several high-resolution, fiber-fed echelle spectrographs and are as follows.

- The Fiber-fed Extended Range Optical Spectrograph (FEROS), being fed with the

2.2m ESO LaSilla telescope (Kaufer et al. 1999) allows one to record in a single exposure the spectral range from 3600 to 9200 Å divided into 39 echelle orders. The resolution of the FEROS spectra is $R=48,000$. FEROS spectral orders cover pretty broad wavelength ranges, which make the spectrograph a very useful tool to check the spectral types and luminosity classes of the observed targets. The measurements are marked as "F" in Table 1.

- The Echelle SpectroPolarimetric Device for the Observation of Stars (ESPaDOnS) spectrograph is the bench-mounted high-resolution echelle spectrograph/spectropolarimeter) attached to the 3.58 m Canada-France-Hawaii telescope at Maunakea (Hawaii, US). It is designed to obtain a complete optical spectrum in the range from 3700 to 10,050 Å. For details see <https://www.cfht.hawaii.edu/Instruments/Spectroscopy/ESPaDOnS/>. The whole spectrum is divided into 40 echelle orders. The resolving power is about 68,000. The spectra from ESPaDOnS were obtained during the runs 05Ao5 (in 2010, with PI: B. Foing) and 15AD83 (in 2015, with PI: G. Walker). The measurements are marked as "E" in Table 1.
- The High Accuracy Radial velocity Planet Searcher (HARPS) spectrograph (Mayor et al. 2003), fed by the 3.6m ESO LaSilla telescope has a resolving power $R=115,000$ and broad spectral range which allows to cover all spectral lines used for classification of stars: HeI, HeII and MgII as well as the interstellar CaII lines. HARPS spectra cover also a vast majority of Diffuse Bands and interstellar molecular features. The measurements are marked as "H" in Table 1.
- BOES (Bohyunsan Echelle Spectrograph) of the Korean National Observatory (Kim et al. 2007) is installed at the 1.8m telescope of the Bohyunsan Observatory in Korea. The spectrograph has three observational modes allowing resolving powers of 30,000, 45,000 and 90,000. In any mode, the spectrograph covers the whole spectral range

from \sim 3500 to \sim 10,000 Å, divided into 75 – 76 spectral orders. The measurements are marked as "B" in Table 1.

It is worth mentioning that all of the above spectrographs are fiber-fed, in most of cases providing an almost excellent flat-fielding procedure. The resulting flat-fielded spectra normally are nearly flat, i.e. the continuum is almost a straight line, making the normalization procedure much more evident than for those of slit instruments in most of cases. This is a very important advantage of fiber-fed spectrographs. Spectra from high-resolution slit spectrographs are often hardly useful for reliable measurements of broad features due to the complex shape (rather crowded) of spectral orders after the flat-field normalization. Also, we used the manual fit procedure to restore the broad DIB profiles, which allows for the elimination of stellar contamination. To confirm the above we present the plot (Fig. 1) comparing the HD204827 spectrum acquired with two fiber-fed echelle spectrographs: BOES and ESPaDOnS. In Fig.4 we show how we measured DIB5780 blended with broad DIB5779: the profile of the broad feature was accepted as a kind of pseudo-continuum. All other blended features were measured in the same manner.

Some objects were observed more than once. For the analysis we have selected the spectra with higher S/N ratio and/or with more evident position of the continuum. The complete set of measured profiles of broad diffuse bands is given in the Appendix.

All spectral images (except the ESPaDOnS data) were processed and measured in standard way using our own DECH¹ code. The spectral resolutions, provided by the above mentioned instruments, are not identical but all are high enough to precisely measure the strengths of the investigated spectral features of atomic and molecular species and, especially, of the broad DIBs.

¹available upon request

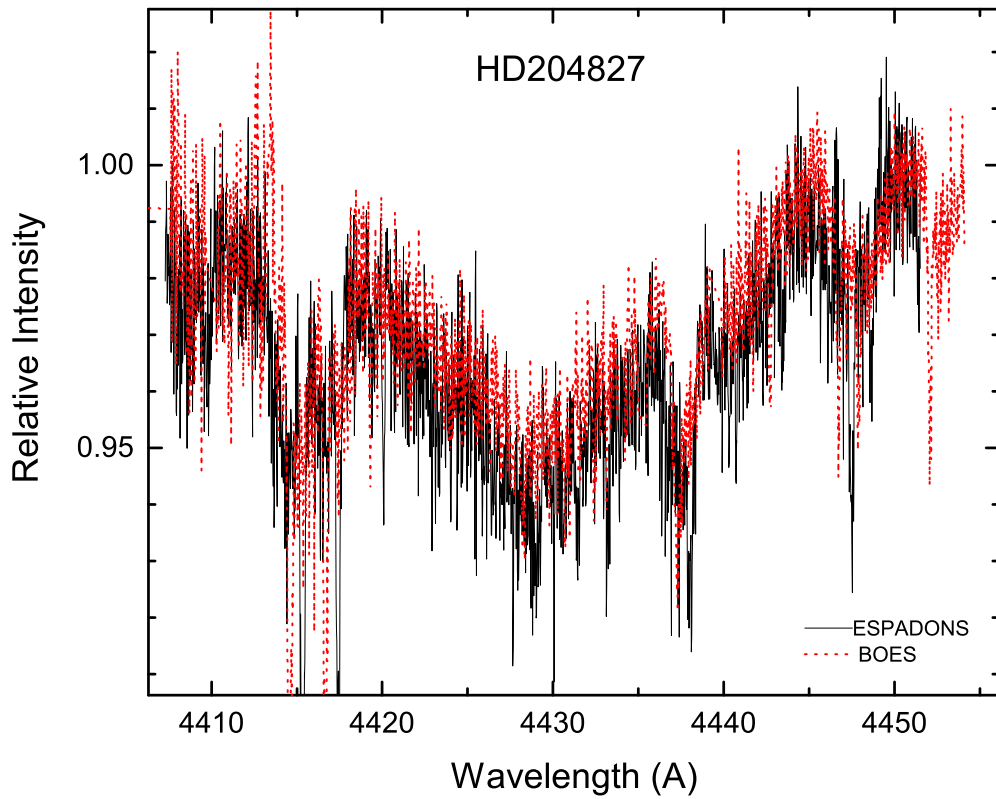


Fig. 1.— Comparison of the 4430 DIB profiles in the spectra from fiber-fed spectrographs ESPaDOnS and BOES. Note their identity inside the apparent noise.

Table 1. Equivalent widths (mÅ) of the confirmed broad DIBs, visible in the spectra of the selected targets, the signal-to-noise ratio (S/N) and FWHM in Å. The selected stars cover a wide range of spectral types (Sp/L = O3I – B8Ib) and reddening ($E(B-V) = 0.28 - 2.01$).

Star	Sp/L	E(B-V)	4428.3 S/N FWHM	4882.0 S/N FWHM	5450.3 S/N FWHM	5779.1 S/N FWHM	6175 S/N FWHM
BD+404220E	O6V	1.96	2700±1300 50 18	4120±940 90 31	560±455 110 17	1143±300 220 16	1988±700 130 30
BD-134923F	O5.5	1.10	1760±490 135 17	1310±450 213 35	375±130 275 14	718±170 290 14	1222±247 290 30
BD-134927F	O7II	0.95	1540±362 135 16	1545±575 195 35	407±185 210 14	870±270 250 19	993±340 176 26
BD-134928F	O9.5V	0.77	1201±460 110 17		395±200 200 13	775±428 160 16	690±337 170 27
BD-134929F	O9V	0.90	1500±421 135 17		356±240 155 14	660±250 230 15	968±317 185 28
CygOB_7B	O3I	1.74	2340±1700 35 17		435±280 120 14	1366±390 130 19	1758±459 170 19
CygOB_8B	O6I	1.58	2160±510 90 16	1100±430 180 20	533±158 270 15	905±230 265 14	1352±240 300 21
CygOB_11B	O5.5I	1.78	2900±900 45 18	1940±630 110 25	456±200 170 14	1040±535 108 13	1982±369 210 22
CygOB_12E	B4Ia	2.01	...			1150±890 65 14	2060±1147 67 29
Hersch36F	O7.5V	0.90	1620±350 190 16		388±74 470 14	1075±364 250 18	392±120 405 20
15785B	B1Iab	0.65	1400±240 250 16	640±220 400 32	323±99 350 13	431±160 370 15	480±180 320 24
24912H	O7.5III	0.31	624±210 220 16		83±78 370 14	215±190 280 15	457±230 290 13
34078B	O9.5V	0.49	760±170 310 19			129±62 800 13	315±226 280 24
73882F	O8.5IV	0.68	840±270 280 15		79±41 680 10	170±120 450 15	460±110 590 22
76341F	O9.2IV	0.51	680±350 180 19		181±104 335 11	130±120 350 12	334±143 360 24
78344F	O9.5Ib	1.32	1906±232 270 16	2580±375 310 33	324±111 325 13	640±137 425 15	987±161 390 21
80077F	B2Ia	1.45	3100±1500 40 19	2890±1200 80 32	400±121 280 12	1243±307 270 17	1230±330 320 26
147165H	B1III	0.34	714±236 220 16			227±67 810 12	
147888F	B3V	0.49	1000±150 510 18		120±50 515 12	514±124 550 17	

Table 1—Continued

Star	Sp/L	E(B-V)	4428.3 S/N FWHM	4882.0 S/N FWHM	5450.3 S/N FWHM	5779.1 S/N FWHM	6175 S/N FWHM
147889H	B2V	1.04	1490±281 280 18		133±45 560 13	652±166 425 17	
148379F	B2Iab	0.74	1665±150 524 16	1600±170 645 34	290±81 670 14	450±108 570 13	370±90 600 19
148937F	O6I	0.65	1218±380 173 17		174±152 240 10	630±308 245 15	809±267 300 26
149038F	O9.7Iab	0.28	1050±160 535 15		127±75 550 13	396±90 940 17	406±136 495 19
149404F	O8.5Iab	0.60	1336±87 800 16	1140±140 720 28	304±109 515 15	592±93 940 15	746±130 500 22
149757H	O9.5V	0.29	120±30 800 9				128±56 600 14
152233F	O6II	0.42	960±300 240 17		174±102 350 13	407±296 290 18	445±90 560 10
152235F	B0.5Ia	0.74	1300±100 650 14	1025±255 460 34	180±122 380 13	457±134 480 15	345±80 570 14
152249F	O9Iab	0.44	1000±190 400 14	535±176 450 25	200±120 422 14	280±102 470 11	485±148 420 17
154368F	O9.5Iab	0.73	850±130 540 17	220±100 560 20	210±56 680 15	354±67 1035 16	457±200 300 18
154445F	B1V	0.35	710±135 550 14			278±121 435 16	110±90 470 14
157038F	B4Ia	0.83	1550±100 690 17	1530±190 560 33	227±92 450 14	413±182 330 12	613±140 460 19
163800H	O7.5III	0.56	700±100 480 14			325±124 470 15	470±97 565 12
166734F	O7.5I	1.34	2560±230 320 17	2105±315 350 33	855±110 490 15	1030±240 360 17	1276±245 360 26
168112F	O5.5	1.00	1880±250 270 17	1145±440 220 31	500±168 330 16	634±165 425 15	1100±170 370 21
168607F	B7Ia	1.55	3100±290 260 18		690±158 310 14	970±205 390 15	1162±230 340 26
168625F	B6Ia	1.47	3100±400 170 16	2570±570 200 35	715±170 290 14	1037±259 290 15	1189±221 290 24
169454F	B4Ia	1.00	1700±350 210 14		360±130 340 14	540±141 440 15	550±168 370 15
179406H	B3V	0.31	420±90 500 14			120±80 650 12	70±43 760 13

Table 1—Continued

Star	Sp/L	E(B-V)	4428.3 S/N FWHM	4882.0 S/N FWHM	5450.3 S/N FWHM	5779.1 S/N FWHM	6175 S/N FWHM
183143E	B6.5I	1.28	3100±390 220 18	2530±230 510 31	640±135 410 15	760±180 320 13	1480±285 350 22 11
185859B	B0.5Ia	0.57	710±130 250 13		360±210 195 14	495±232 325 20	351±210 270 20 11
204827B	O9.5IV	1.07	750±260 175 13		350±150 220 13	233±262 230 16	380±375 150 22
208501B	B8Ib	0.63	740±310 160 16		305±145 200 13		
319703F	O6	1.50	2310±380 190 17	2390±560 200 38	410±125 300 14	1128±293 302 14	1320±205 300 26

3. Results

Values of the equivalent widths for DIBs and column densities for KI and CH are presented in Tables 1 and 2. The equivalent width errors were estimated using the method from Vollmann & Eversberg (2006) in which both spectral noise and uncertainty of the continuum normalization are taken into account.

Sonnentrucker et al. (2018) mention many very broad DIBs but only some of them are marked as confirmed. Let's consider one example marked by (Sonnentrucker et al. 2018) as probable: the 6311 DIB was originally mentioned by (Herbig 1975) as a broad unconfirmed feature seen in HD183143. However, there are no data for this DIB in the measurements given in table of (Herbig 1975). Then, in Jeniskens & Desert (1994) the feature is marked as present, however profiles in Fig. 6 (page 65 in the cited article) hardly prove this statement. Nevertheless, Tuairisg et al (2000) measured the feature as 6311.53 in HD183143, BD+40 4220 and BD+63 1964 though without addressing the stellar and interstellar contamination effects, which are severe in this area. Indeed, our spectra of the latter two objects do not confirm the presence of any broad feature in this area while the available spectra of HD 183143 cannot prove or disprove the presence of 6311.53 DIB due to the stellar contamination and continuum normalization issues. In our plot (Fig. 2) we clearly demonstrate that the suspect DIB is a stellar HeII line, typically observed in O-type stars. The feature does not exist in HD147889 as the latter is of B3V Sp/L, despite a very high reddening. In the upper panel of Fig. 2 we provide a comparison with the synthetic spectra calculated by Lanz & Hubeny (2003) and Lanz & Hubeny (2007) freely available in the TLUSTY web page¹. The shown stellar lines' identification is based on the VALD database (Piskunov et al. 1995) line lists compiled with the effective temperature and logarithm of gravity values indicated for each synthetic spectrum in Figure 2.

¹<http://nova.astro.umd.edu/Tlusty2002/tlusty-frames-models.html>

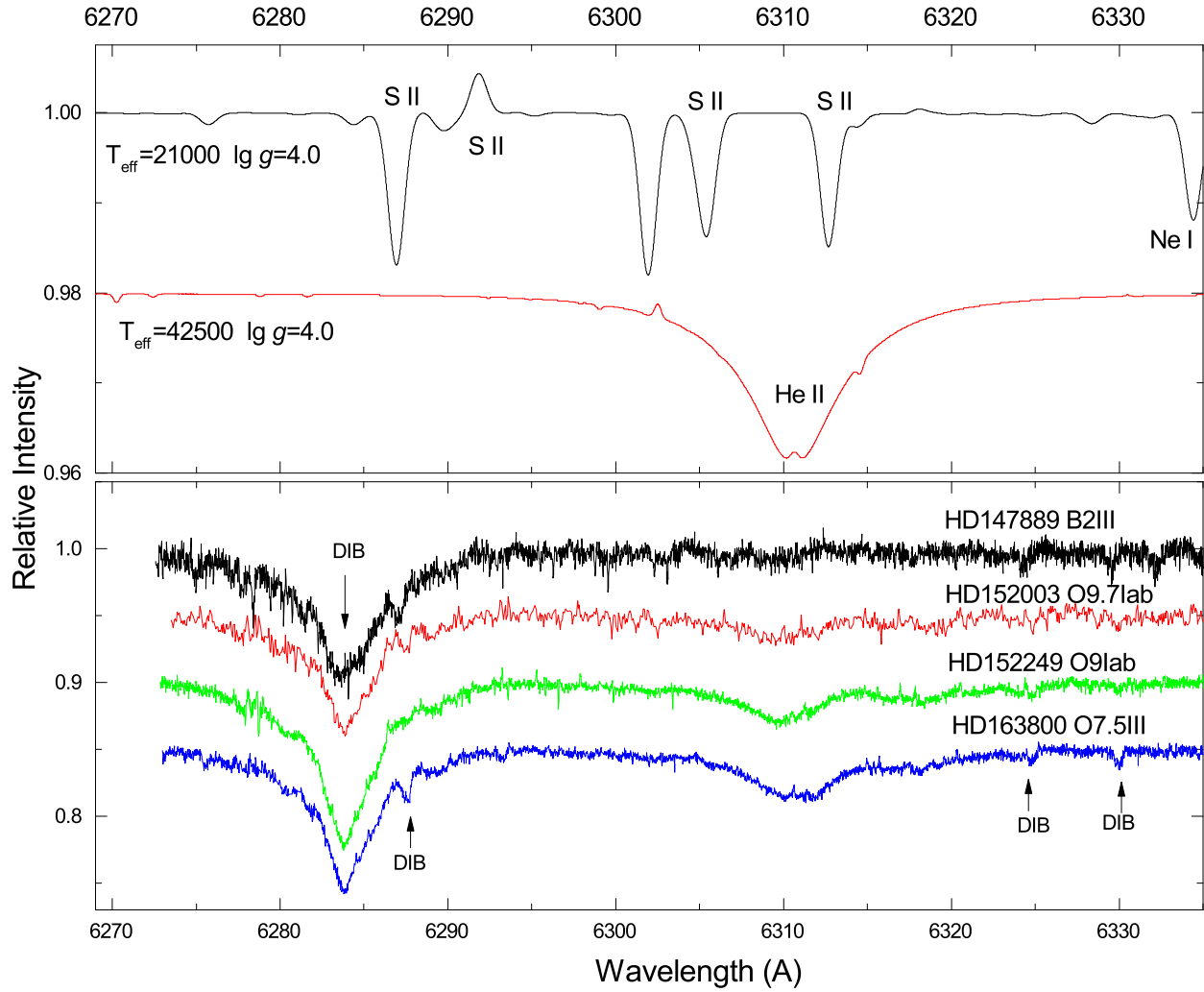


Fig. 2.— The feature mentioned as possible 6311 DIB in work by Sonnentrucker et al. (2018) is, in fact, a stellar HeII line, characteristic for O type stars (see text). As the ion line it is especially strong in supergiant spectra.

The 4882 feature is among the very broad DIBs, mentioned by (Herbig 1975). Its measurements are naturally difficult because of the close proximity of the stellar H_{β} line. This explains why the number of measurements of this feature given in Table 1 is substantially reduced. Worth mentioning is the rather poor correlation between this diffuse band and the amount of dust particles, which is demonstrated in Figures 3 and 8.

To verify what has been measured in our spectra, we show the profiles of our confirmed very broad DIBs (Fig. 4). To extract the profiles we have selected a very heavily reddened O7.5Iab star, HD166734, where the stellar contaminations in the DIB profiles are the smallest. It is of importance to mention that, e.g. the profile of the 6175 DIB, presented by Sonnentrucker et al. (2018) in the spectrum of B7 supergiant HD183143, is likely shown as too broad, perhaps because of stellar contaminations in its blue side. In all our spectra of O-type stars the profile begins around 6155 Å, not around 6130 Å. This is the possible source of errors: the borders of very broad features are ill-defined. It is thus very important to compare the spectra of different spectral types taken using different instruments.

Our measurements of the sample of 43 high-resolution, high-S/N ratio spectra do confirm the already reported (see the Introduction) correlations of the very broad DIBs with a color excess; Figs. 7, 8 present the least-squares linear fits and the correlation coefficients for broad DIBs. All calculations were performed with the Y-errors taken into account.

We have measured the EWs of the broad DIBs (see Table 1), fitting the profile manually to separate the stellar contaminations (Herbig (1966); Krełowski et al. (1987)), especially strong in B type stars. Such a procedure leaves some arbitrariness but a more precise method hardly exists as the stellar spectra are a bit unpredictable (see an example of measurements in Fig. 5). This may lead to a correlation coefficient a bit smaller than the true one. In any case the broad features 4430, 6175 and 5779 do correlate quite tightly with E(B–V) while 4882 and 5450 demonstrate a lower magnitude of correlation with the

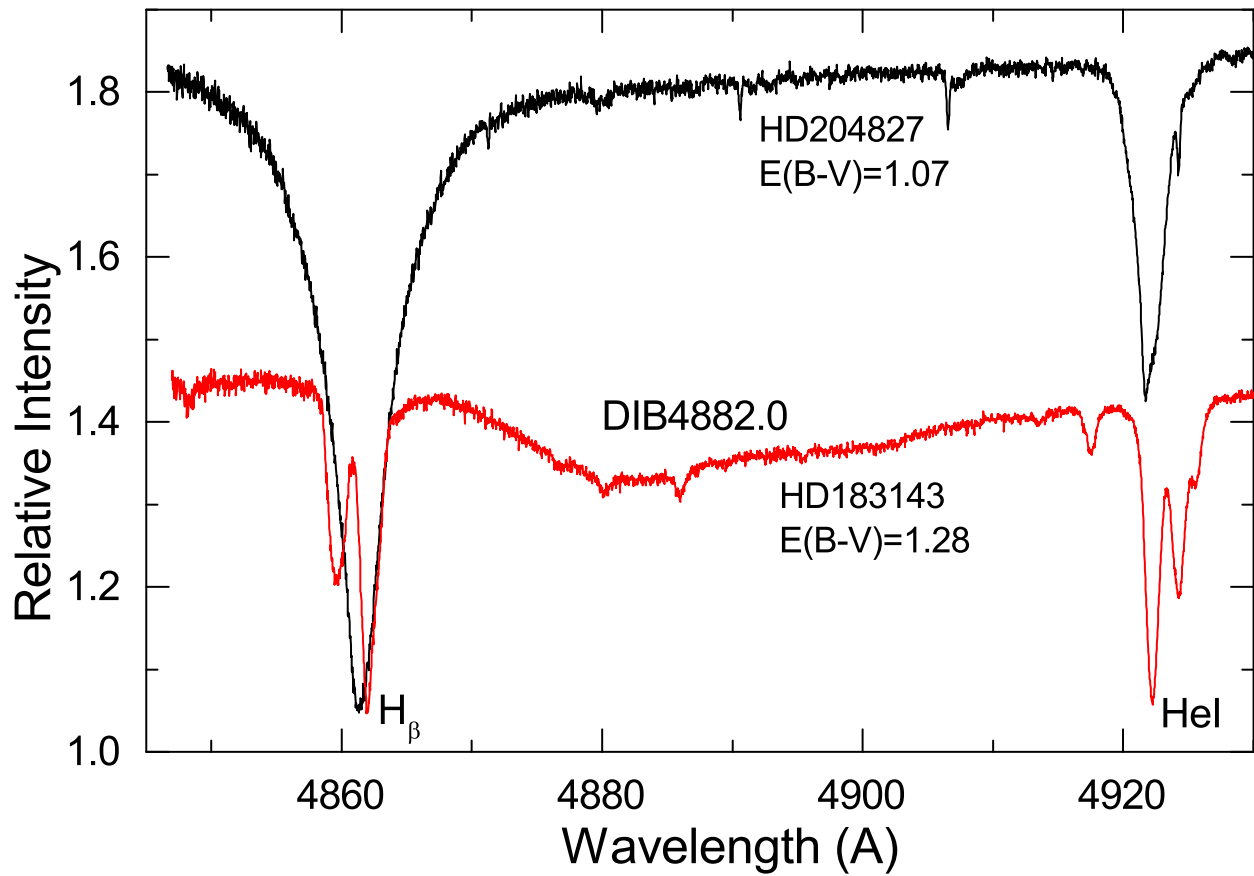


Fig. 3.— Fragments of two spectra of heavily reddened stars, covering the 4882 very broad DIB. Note the lack of the simple relation of the DIB to $E(B-V)$.

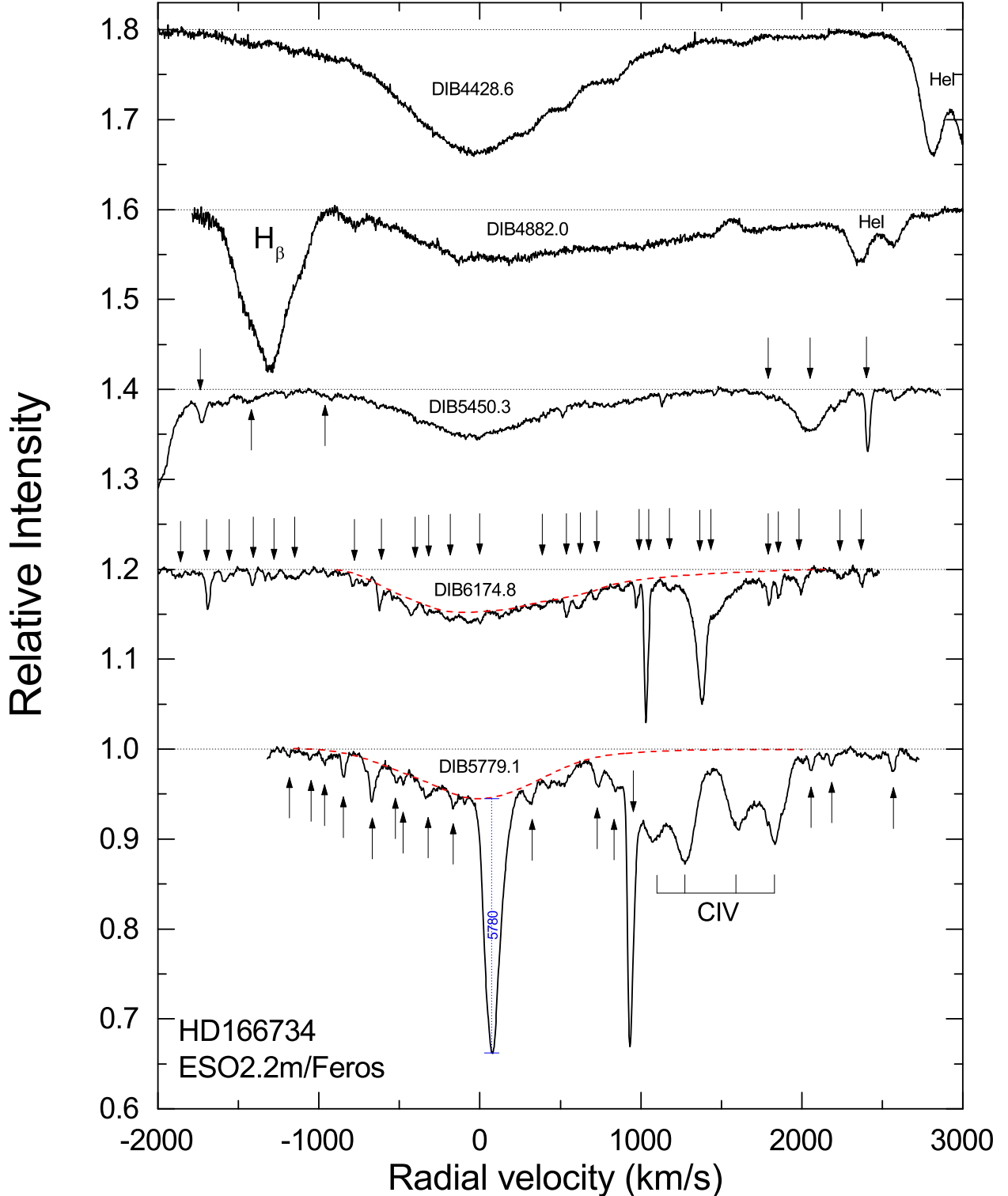


Fig. 4.— Profiles of the confirmed broad DIBs in the spectrum of hot binary O star. Arrows mark the narrow diffuse bands. Dash lines show profiles of broad DIBs 6175 and 5779. Note the vertical span of DIB 5780 representing how we measure this feature.

amount of interstellar dust.

Some diffuse bands are severely contaminated by telluric lines, e.g. reasonably broad DIB6284. Fortunately, spectra from fiber-fed spectrographs provide almost excellent removal of telluric lines by means of telluric standard stars. A good example is given in Fig. 6.

One of the very broad features, depicted at Fig. 4, is the 5450 DIB. It is reasonably weak and its profile is contaminated with stellar lines in B-type stars. The above makes the measurements of EWs uncertain. This is why a correlation between this DIB and $E(B-V)$ is lower than that of DIBs 4430, 6175, and 5779 (see Fig. 7).

A closer look into the area around 6175 reveals that the observed broad feature is a blend of at least two also broad bands centered approximately at 6170 and 6177 Å. Sometimes this separation is quite evident due to deep 6170 DIB: Cyg OB2 objects, HD 152233, HD 154368, HD 163800, etc. However, e.g. BD-13 4923, BD-13 4928, BD-13 4929, HD73882, HD319703, etc. exhibit a rather smooth profile without any indications of the presence of the blend.

It is particularly surprising that very broad 6175 DIB is pretty tightly correlated with $E(B-V)$ (Fig. 7). Despite a possible source of uncertainty, due to the manual fit and the abovementioned issues, the correlation coefficient is as high as 0.89. Thus the carriers of the very broad DIBs seem to be well mixed with other interstellar species, including dust grains. The correlation, based on our sample of 40 high-resolution, high-S/N ratio spectra, looks tighter than those presented by Sonnentrucker et al. (2018). The correlation would be even tighter but HD204827 departs down from the average relation and this effect is certainly not due to a measurement error.

Sonnentrucker et al. (2018) tried to relate the very broad diffuse band 6177 (we mark

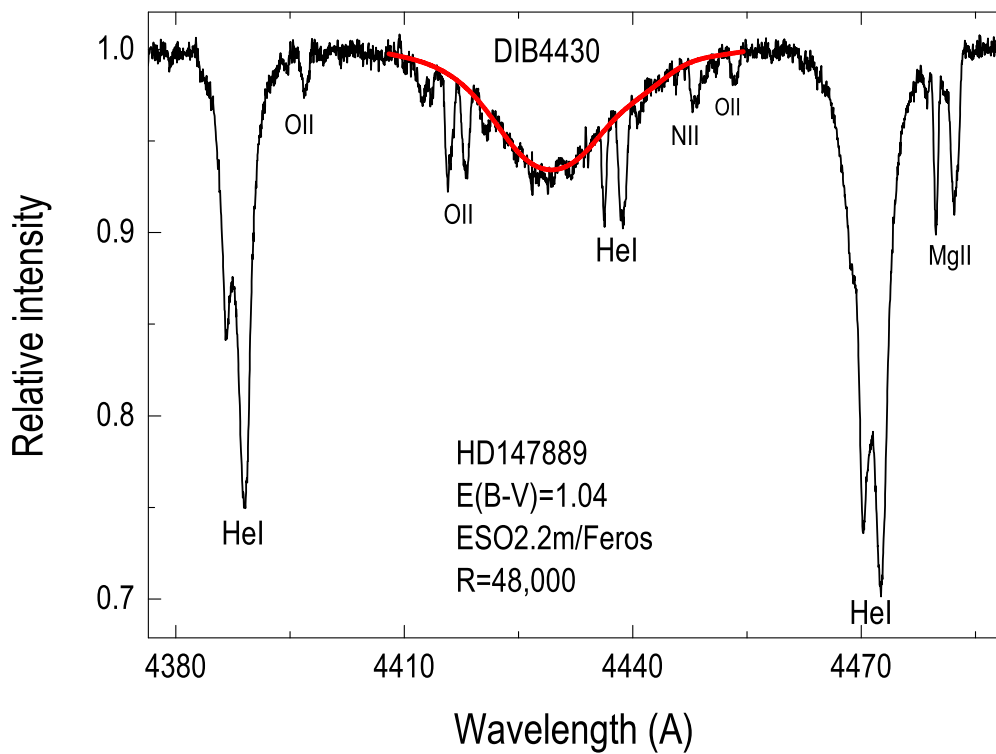


Fig. 5.— Example of the measurement of the broad (FWHM 18 Å) DIB4430 with the manually fitted profile overplotted on the original spectrum.

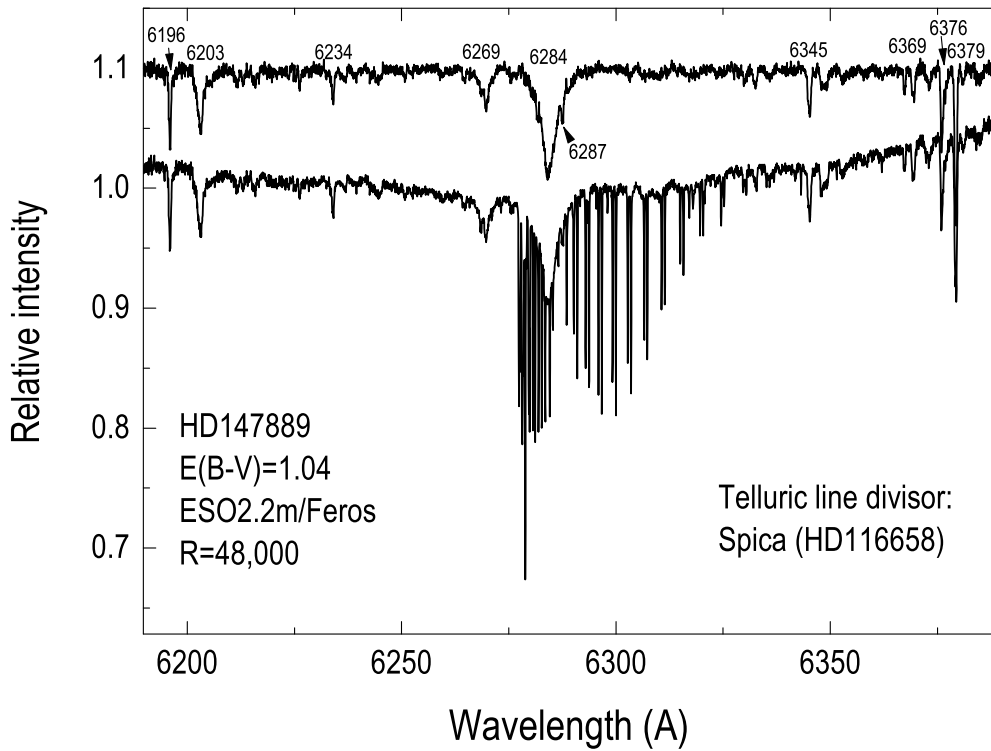


Fig. 6.— Example of telluric lines removal from the profile of broad DIB 6284. Narrow DIBs are also marked. The lower spectrum is a raw data just normalized to just one point for clarity.

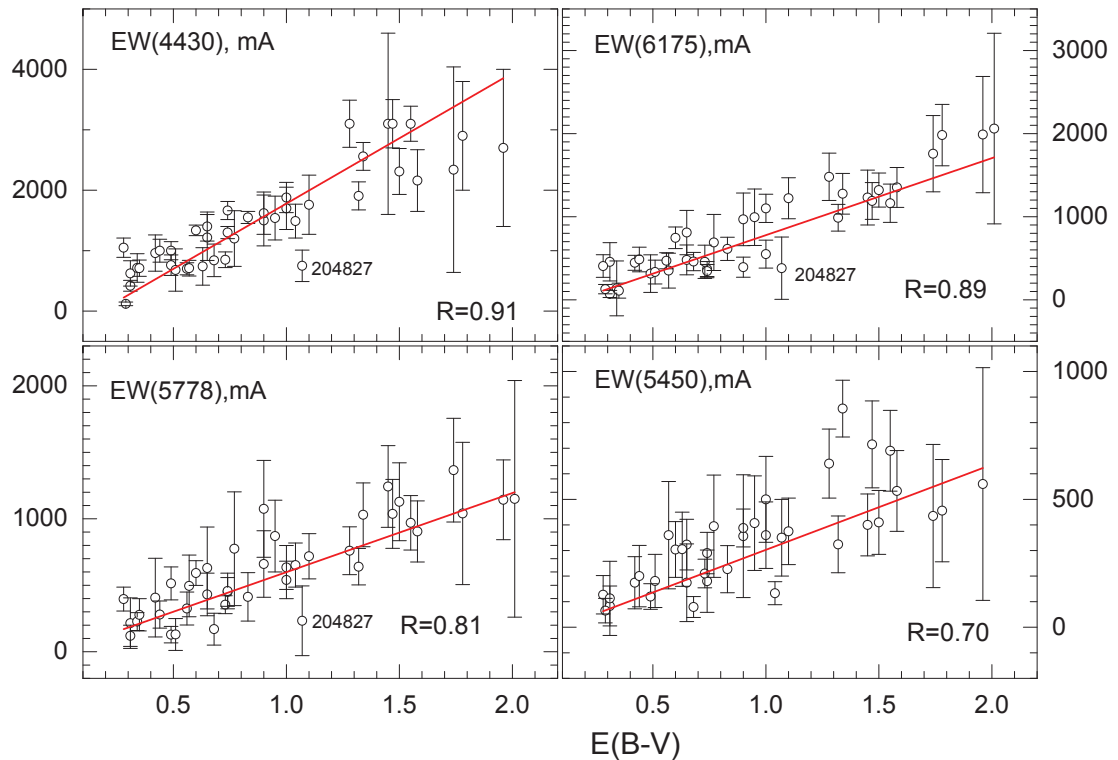


Fig. 7.— Weighted linear fits with reasonably tight correlations between EWs of four very broad DIBs and $E(B-V)$.

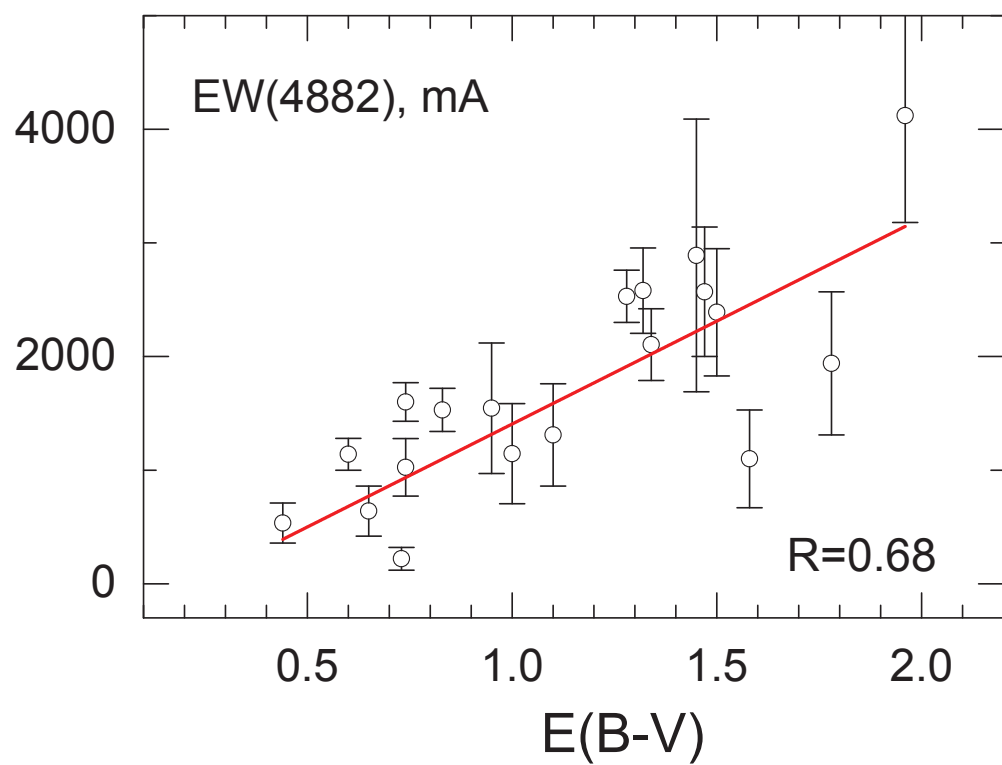


Fig. 8.— Weighted linear fits between EWs of 4882 DIB and $E(B-V)$.

it as 6175) to other, narrower ones, in particular DIB 5780. The latter is the major one, discovered by Heger (1922). Both features in the Figure 10 of Sonnentrucker et al. (2018) seem to be closely related but the observed scatter seems to exceed the measurements' errors.

We have also checked the interrelations between very broad and narrower DIBs. The weighted linear fits with Pearson's correlation coefficients are depicted on Fig. 9. The correlations' magnitudes were calculated with measurement errors taken into account as the weights. All the fits presented on the Fig. 9 have the slope's standard error between 0.07 and 5.05: with their best value (0.07) for the relation 6175 vs 6284 DIB and the worst one (5.05) for the relation 6175 versus 4963 DIB.

It is evident that the blend of broad DIBs at 6175 correlates very well with DIBs 5780, 6614 and, especially with 6284, which supposes a similar physical environment for their carriers. Its correlation with the narrow 4963 DIB is not so tight. It is, however, much more evident than that presented by Sonnentrucker et al. (2018). Let's emphasize that our sample is twice as big as that in the latter paper. Anyway, the mutual correlations between the abovementioned DIBs are never as tight as that between 6614 and 6196 DIBs (Krełowski et al. 2016).

Sonnentrucker et al. (2018) divided the observed DIBs into the sets related to either atomic or molecular gas. The last one was considered as the environment for the 4963 DIB carrier. To verify this we related the column densities of the KI 7699 Å line and the CH 4300.3 Å molecular feature to this band strength. Weighted fits, shown in Fig. 10, have the slope's standard error 0.06 for K column densities versus 4963 EWs and 0.19 for CH column densities versus 4963 EWs. As seen in Fig. 10 the 4963 DIB correlates better with the atomic feature than with the molecular one. The former would be much better if not the specific object — HD147889. It is hard to say why the KI line is so weak in the spectrum

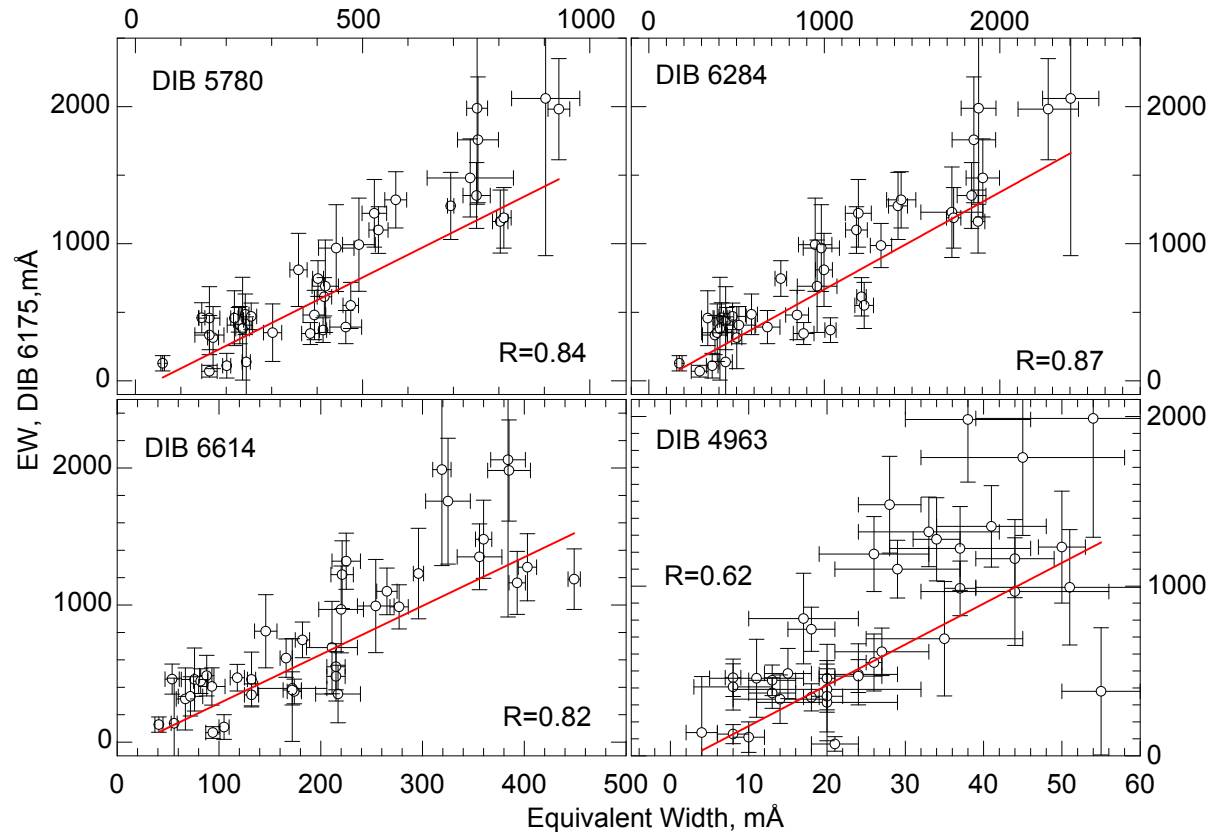


Fig. 9.— Correlation of broad 6175 DIB with other, narrower diffuse bands with tight correlation between the very broad 6175 DIB and the much narrower 5780 and 6284 ones. Apparently their carriers are to be found in the same environments.

of this star. It was, however, verified in a few spectra from different instruments and thus is real. Anyway Fig. 10 creates some doubts on whether the 4963 carrier is really situated in molecular gas rather than in atomic gas. On the other hand, Thorburn et al. (2003) marked DIB 4963 as so-called C₂-DIB correlating with the abundance of the interstellar C₂ molecule. However, this conclusion was questioned by Galazutdinov et al.(2006) where the authors estimated the correlation coefficient as low as 0.56 for 20 measurements. Recently, Elyajouri et al. (2018) estimated the correlation between intensities of 18 C₂-DIB including DIB 4963 and reported the correlation level for it as high as 0.95. The estimation is based on a rather small number of measurements thus the significance of the attribution of DIB 4963 as a C₂-DIB remains low.

In Fig. 11 we provide the general average of all measured profiles of broad diffuse bands with estimated FWHM and the rest interstellar wavelength position. A good question is: where is the center of very asymmetric DIB4882? As it is shown in Fig. 11, we attributed the rest wavelength position to the deepest part of the feature's profile, namely at 4882.0 Å. Thus, this diffuse band is a holder of a very extended right (red) wing with a rather sharp cut on the left (blue) wing that mimics the behavior of well-known bands of simple molecules. The average FWHM of this band, 32 Å makes it the broadest feature of the sample. Other bands' central wavelengths and FWHM (given in the parentheses) are 4428.6 (17 Å), 5450.3 (14 Å), 5779.1 (16 Å) and 6174.8 (25 Å). The variability of the FWHM from object to object (Table 1) can be explained by the following reasons: (i) due to the shallowness of the broad features, the FWHM is very sensitive to the continuum normalization uncertainties and the position of the deepest point of the profile. The situation is more complex if the S/N ratio is low and in cases of severe stellar contamination. (ii) The FWHM may grow with the increasing the number of populated transitions of carrier molecule, i.e. the variability of the FWHM may be of physical origin.

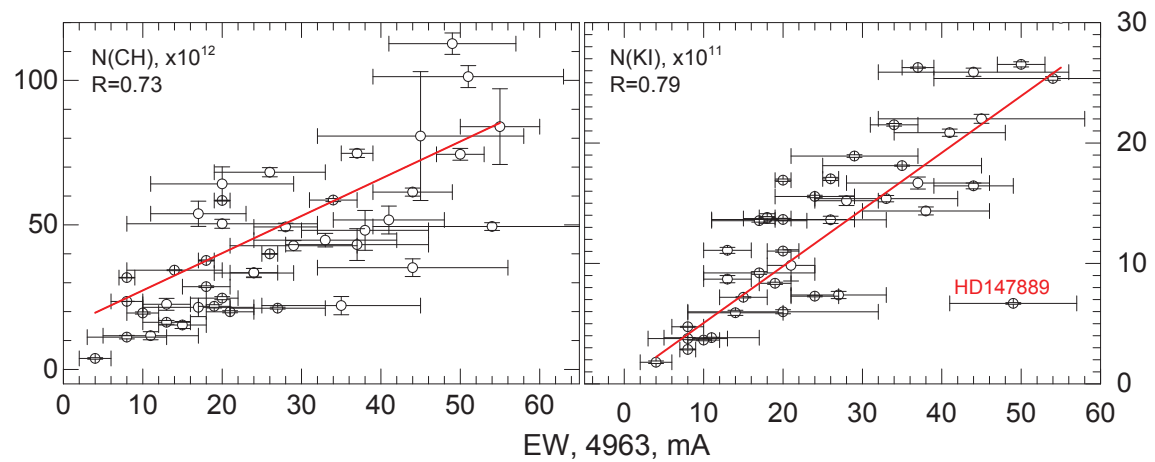


Fig. 10.— Correlation of DIB 4963 with CH and K. There is no evidence that the DIB originates in molecular clouds.

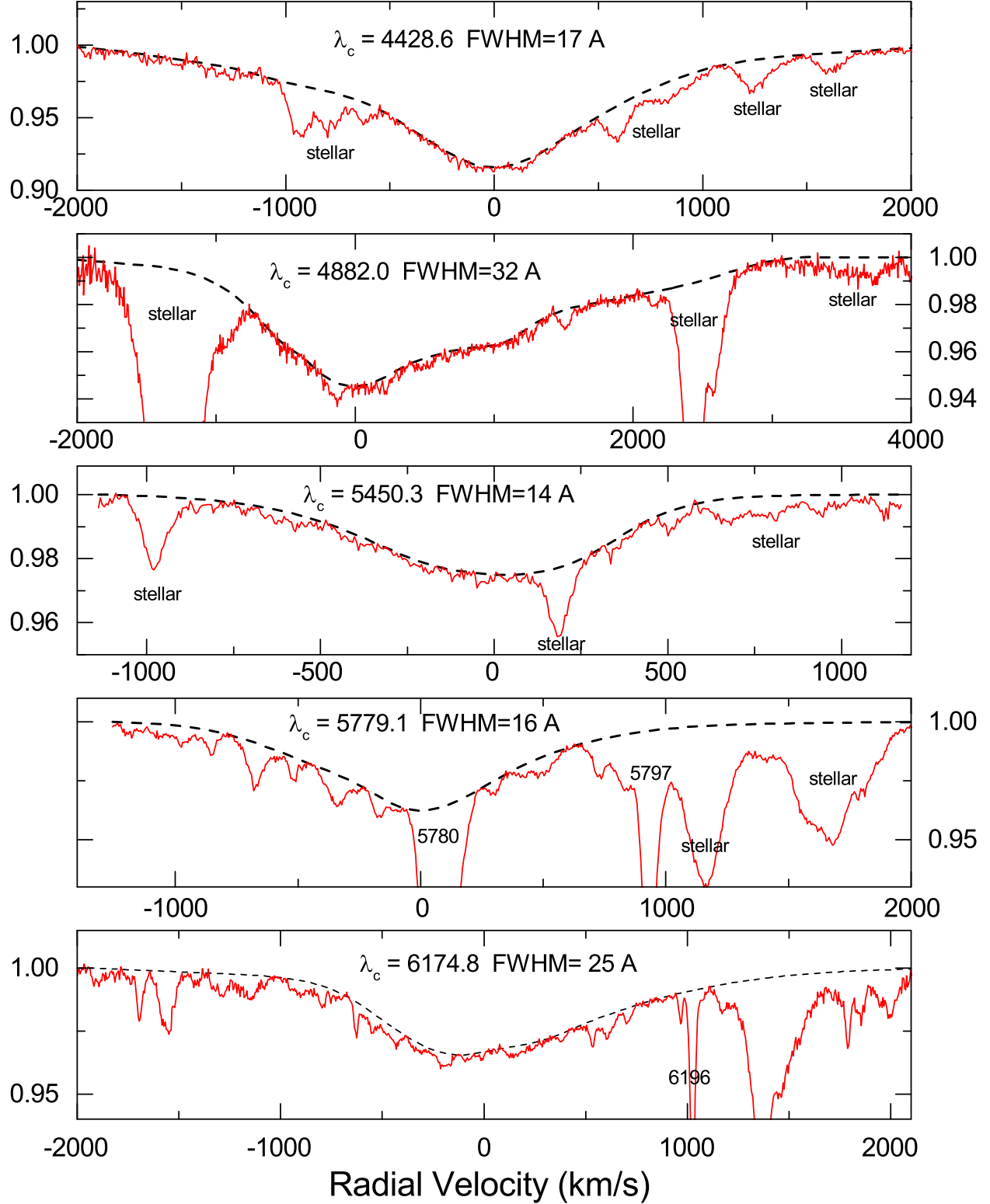


Fig. 11.— General average of the profiles of studied DIBs in the interstellar radial velocity scale with estimated rest wavelength and FWHM. All unmarked absorptions are diffuse bands; see Fig. 4.

Table 2. Equivalent widths (mÅ) of some relatively narrow DIBs, including weak band at λ 4963 Å one of so-called C₂ DIBs (Thorburn et al. 2003), and column densities (cm⁻²) of CH and KI.

Star	EW(4963)	EW(5780)	EW(6284)	EW(6614)	N(CH)×E12	N(KI)×E11
BD+404220	54±15	752±23	1879±99	319±9	49.44±1.34	25.36±0.15
BD-134923	37±9	526±27	1194±74	221±11	43.19±5.49	16.68±0.50
BD-134927	51±12	492±36	948±95	254±18	101.3±3.80	30.99±0.35
BD-134928	35±10	418±29	959±113	211±25	22.08±3.16	18.12±0.05
BD-134929	44±12	442±39	983±103	220±22	35.21±3.06	25.88±0.34
CygOB_7	45±13	754±45	1852±124	325±22	80.74±22.29	22.01±0.37
CygOB_8	41±7	751±30	1839±82	356±22	51.70±4.80	20.86±0.30
CygOB11	38±8	932±24	2276±172	385±21	48.11±6.90	14.36±0.33
CygOB12	...	903±75	2404±160	384±17	...	46.47±0.34
Hersch36	20±12	463±35	676±71	172±34	50.40±1.56	5.99±0.17
15785	24±5	394±25	845±65	215±9	33.35±1.58	15.56±0.10
24912	11±6	163±23	438±12	76±13	11.67±1.39	3.84±0.03
34078	20±9	171±12	501±29	67±9	64.20±5.88	13.65±0.10
73882	8±1	146±7	414±48	54±7	31.75±0.11	2.86±0.04
76341	14±6	163±32	377±71	72±12	34.33±0.15	5.90±0.21
78344	37±2	...	1323±61	277±9	74.78±1.43	26.26±0.05
80077	50±3	...	1727±177	296±5	74.44±2.04	26.53±0.21
147165	4±2	244±9	438±38	56±3	3.81±0.27	1.80±0.10
147888	19±2	248±22	267±87	83±13	21.84±0.57	8.35±0.09
147889	49±8	371±13	435±22	179±9	112.70±3.71	6.68±0.07
148379	13±3	413±8	1035±32	174±7	22.53±2.06	11.09±0.25
149038	8±5	230±28	513±96	93±13	11.16±0.60	3.76±0.09
149404	18±3	402±12	752±33	182±7	28.63±0.32	13.73±0.40
148937	17±7	359±19	998±48	146±11	21.47±3.18	9.21±0.11
149757	8±2	60±4	174±15	41±4	23.52±0.04	4.74±0.04

Table 2—Continued

Star	EW(4963)	EW(5780)	EW(6284)	EW(6614)	N(CH)×E12	N(KI)×E11
152233	13±3	227±11	444±40	82±7	16.30±0.65	8.70±0.30
152235	18±1	385±19	882±59	132±7	37.70±0.20	13.82±0.07
152249	15±3	242±8	585±34	88±7	15.36±1.22	7.19±0.05
154368	20±1	218±8	336±36	132±4	58.45±0.10	16.91±0.10
154445	10±2	201±9	361±33	105±5	19.53±0.39	3.64±0.06
157038	27±6	416±16	1212±27	166±6	21.20±0.31	7.38±0.30
163800	24±3	255±12	477±78	118±7	33.46±1.48	7.28±0.05
166734	34±3	694±7	1420±54	403±9	58.60±0.52	21.51±0.11
168112	29±8	535±21	1183±62	265±10	42.80±1.77	18.92±0.11
168607	44±5	803±17	1876±39	393±8	61.36±1.41	16.44±0.24
168625	26±7	811±16	1737±41	449±6	68.24±1.58	13.62±0.30
169454	26±1	474±17	1227±53	215±9	39.96±0.11	17.02±0.13
179406	21±3	163±17	290±48	94±7	19.95±0.36	9.84±1.30
183143	28±4	737±95	1903±95	360±8	49.30±1.29	15.21±0.40
185859	20±2	302±20	390±89	217±22	24.67±0.52	11.03±0.10
204827	55±5	236±15	405±39	172±9	84.00±13.10	30.35±0.20
208501	17±6	248±38	524±95	129±12	53.86±4.36	13.55±0.12
319703	33±9	573±24	1438±83	225±14	44.74±2.34	15.38±0.26

4. Discussion

Our conclusions do not always agree with those of Sonnentrucker et al. (2018). In many cases we can confirm the latter: most of the mutual correlations between different DIBs look very similar. Thus we confirm the existence of strong correlation between a broad 6175 DIB and two medium 5780 and 6284 ones where the Pearson correlation coefficients are 0.84 and 0.87, respectively. This may confirm that they have the same molecular carrier (McCall et al. 2010). It is worth mentioning that our paper (Krełowski et al. 2016) demonstrates examples of evidently different 6196 vs. 6614 strength ratios and thus it is difficult to state that any two DIBs are of common origin.

However, we do not confirm a poor correlation (between the 6175 DIB and $E(B-V)(r=0.57)$ of Sonnentrucker et al. (2018) versus $r=0.89$ in the present paper, as well as too low of a degree of correlation ($r = 0.01$ in Sonnentrucker et al. (2018)) between 6175 and 4963 DIBs, it is 0.62 in our case.

It is also rather risky to divide the observed DIBs in between of atomic and molecular gas clouds. It is clear from Fig. 10 for the case of the relatively weak and narrow diffuse band at $\lambda 4963 \text{ \AA}$, so-called C₂ DIB. The figure demonstrates a better relation between this DIB and the atomic KI, not the CH molecule, as it could be inferred, e.g. from the Sonnentrucker et al. (2018), where, on the basis of poor correlation between the 6175 and 4963 diffuse bands, the authors suggest an atomic gas environment for DIB 6175.

The current list of the observed molecules in ISM is available at <https://www.cv.nrao.edu/~{}awootten/allmols.html>. The most numerous group among them are two- and three-atomic molecules. An attempt to fit vibrational contours of the molecules to the very broad DIBs results in the following assumptions:

1. $4430 \rightarrow \text{CuCl D}^1\Pi - \text{X}^1\Sigma (0, 1)$ medium-strong band with a red-degraded double head

at 4433.8; $4881 \rightarrow \text{CuCl } \text{B}^1\Pi-\text{X}^1\Sigma$ (0, 0) strong band with a red degraded head at 4881.5. It is very interesting that the CuCl bands occur rather frequently as impurities in other spectra, especially in flames, fluorescence, absorption, discharge tubes, and also in arc. They also appear when CuCl is introduced into active nitrogen (Rao, Asundi & Brody 1962); however, the very low abundances of both elements make this hypothesis uncertain.

2. $5450 \rightarrow \text{BO}_2$, headless and narrow band (maximum intensity at 5450). The waves of the bands are observed when boric acid is introduced into an arc or flame, or when finally divided boron is burnt (Kasan & Milliken 1961); once again the abundance of boron makes the hypothesis unlikely.
3. $5779 \rightarrow \text{SrF}$, yellow system ($\text{B}^2\Sigma^+-\text{X}^2\Sigma^+$) (0, 0) band with a close double heads at 5779.5 in *Q* branch and 5772.0 in *R* branch (Novikov & Gurvich 1967); it also looks like a chance coincidence of spectral features since the abundances of strontium and fluor are very rare in the space;
4. $6175 \rightarrow \text{FeO}$, orange (A0, 2ii) strong band of A system (red degraded head at 6180.5) (Pears & Gaydon 1984). In this case both elements are quite abundant which makes this hypothesis much more likely than the former ones.

Among them, only the existence of the FeO molecule has been confirmed in the ISM (<https://cdms.astro.uni-koeln.de/cdms/portal/>). Also, the abundance of oxygen and iron is quite high in comparison to rather exotic other elements listed in the first three cases. Thus only the last item may have some real meaning. Thus the molecular spectroscopy in its present state gives us no suggestion as to what the carriers of broad DIBs may be.

J.K., R.H. and W.S. acknowledge the financial support of the Polish National Science

Centre under the grant 2017/25/B/ST9/01524 for the period 2018 – 2021. G.G. and J.K. acknowledge the financial support of the Chilean fund CONICYT grant REDES 180136.

REFERENCES

- Beals, C. S. & Blanchet, G. H. 1938, MNRAS, 98, 398
- Cordiner, M. A., Linnartz, H., Cox, N. L. J. et al. 2019, ApJ, 875, 28
- Danks, A.C., 1980, PASP, 92, 52
- Dekker, H., D'Odorico, S, Kaufer, A., Delabre, B. & Kotzlowski, H., 2000, Proc. SPIE 4008, p. 534
- Elyajouri et al. 2018, A&A, 616, 143
- Fan H., Hobbs L.M., Dahlstrom J.A., Welty D.E., York D.G., Rachford B., Snow T.P., Sonnentrucker P., Baskes N., Zhao G., 2019, ApJ, in press
- Galazutdinov, G. A., Musaev, F. A., Krelowski, J., Walker, G. A. H., 2000, PASP, 112, 648
- Galazutdinov, G. A., Lee, Jae-Joon, Han, Inwoo, Lee, Byeong-Cheol, Valyavin, G. & Krelowski, J. 2017, MNRAS, 467, 3099
- Galazutdinov, G. A., Shimansky, V. V., Bondar, A. et al. 2017, MNRAS, 465, 3956
- Galazutdinov, G. A.; Krelowski, J., 2017, Acta Astronomica, 67, 2, 159
- Gammelgaard, P., 1975, å, 43, 85
- Greenstein, J. L. & Aller, L. H., 1950, ApJ, 111, 328
- Heger, M. L. 1922, Lick Obs. Bull., 10, 146
- Herbig, G. H., 1966, Z. fuer Ap., 64, 512
- Herbig, G.H. 1967, IAUS, 31, 85
- Herbig, G.H. 1975, ApJ, 196, 129

M. Hobbs, D. G. York, T. P. Snow, et al., 2008, ApJ, 680, 1256

Houziaux, L., Nandy, K. & Morgan, D. H., 1980, MNRAS, 138, 495

Isobe, S., Sasaki, G., Norimoto, Y. & Takahashi, J. 1986, PASJ, 38, 511

Jenniskens, P.; Desert, F. -X. 1994, A&AS, 106, 39

Kasan, W. E. and Milliken, R. C., 1961, J. Chem. Phys. 39, 1738

Kaufer, A. et al. 1999, The Messenger 95, 8

Kim, K.-M., Han, I., Valyavin, G. G., et al. 2007, PASP, 119, 1052

Krełowski J., 2018, PASP, 130, 1001

Krełowski, J., Galazutdinov, G. A., Strobel, A. & Mulas, G., 2016, Acta Astronomica, 66, 469

Krełowski, J., Galazutdinov, G. A., Bondar, A. & Beletsky, Y., 2016, MNRAS, 460, 2706

Krelowski, J., Walker, G. A. H., Grieve, G. R. & Hill, G. M. 1987, ApJ, 316, 449

Lanz, T.; Hubeny, I., 2003, ApJS, 146, 417

Lanz, T.; Hubeny, I., 2007, ApJS, 169, 83

Mayor, M., Pepe, F., Queloz, D., Bouchy, F. et al. 2003, The Messenger 114, 20

McCall, B. J., Drosback, M. M., Thorburn, J. A., York, D. G., Friedman, S. D., Hobbs, L. M., Rachford, B. L., Snow, T. P., Sonnentrucker, P., Welty, D. E., 2010, ApJ, 708, 1628

Merrill, P. W., Humason, M. L., 1938, PASP, 50, 212

Novikov, M. M. and Gurvich, L. V., 1967, Opt. Spectrosc., 22, 395

Pears, R. W. B and Gaydon, A. G., “The Identification of Molecular Spectra”, Chapman and Hall, London, New York, 1984

Piskunov et al., 1995, A&AS, 112, 525

Rao, P. R., Asundi, R. K. and Brody, J. K., 1962, Canad. J. Phys., 40, 42 and 1443

Rudkjøbing, M., 1970, Ap&SS, 6, 157

Sonnentrucker, P., York, B., Hobbs, L. M., Welty, D. E. et al. 2018, ApJS, 237, 40

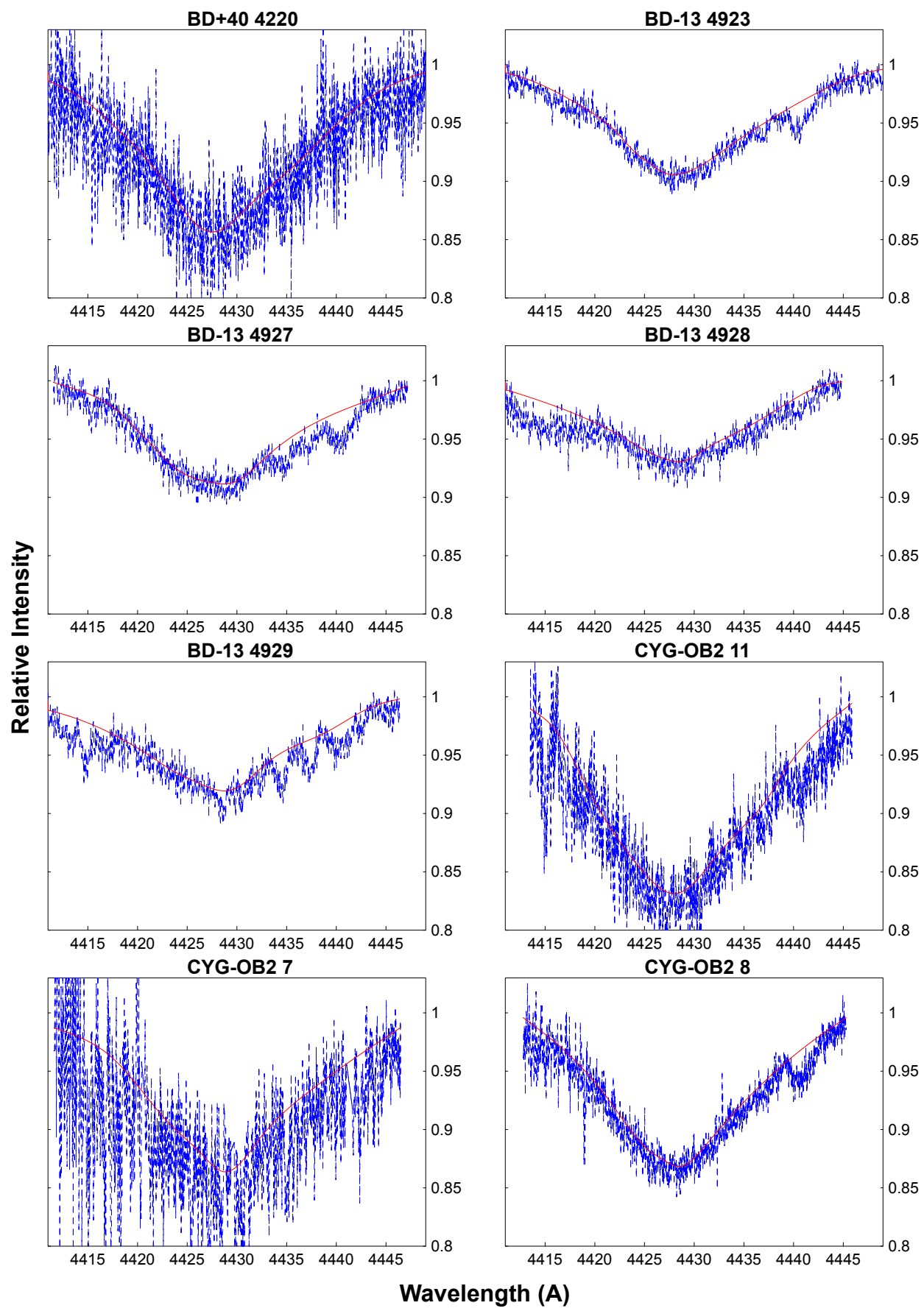
Thorburn, J. A., Hobbs, L. M., McCall, B. J., Oka, T., Welty, D. E., Friedman, S. D., Snow, T. P., Sonnentrucker, P., York, D. G., 2003, ApJ, 584, 339

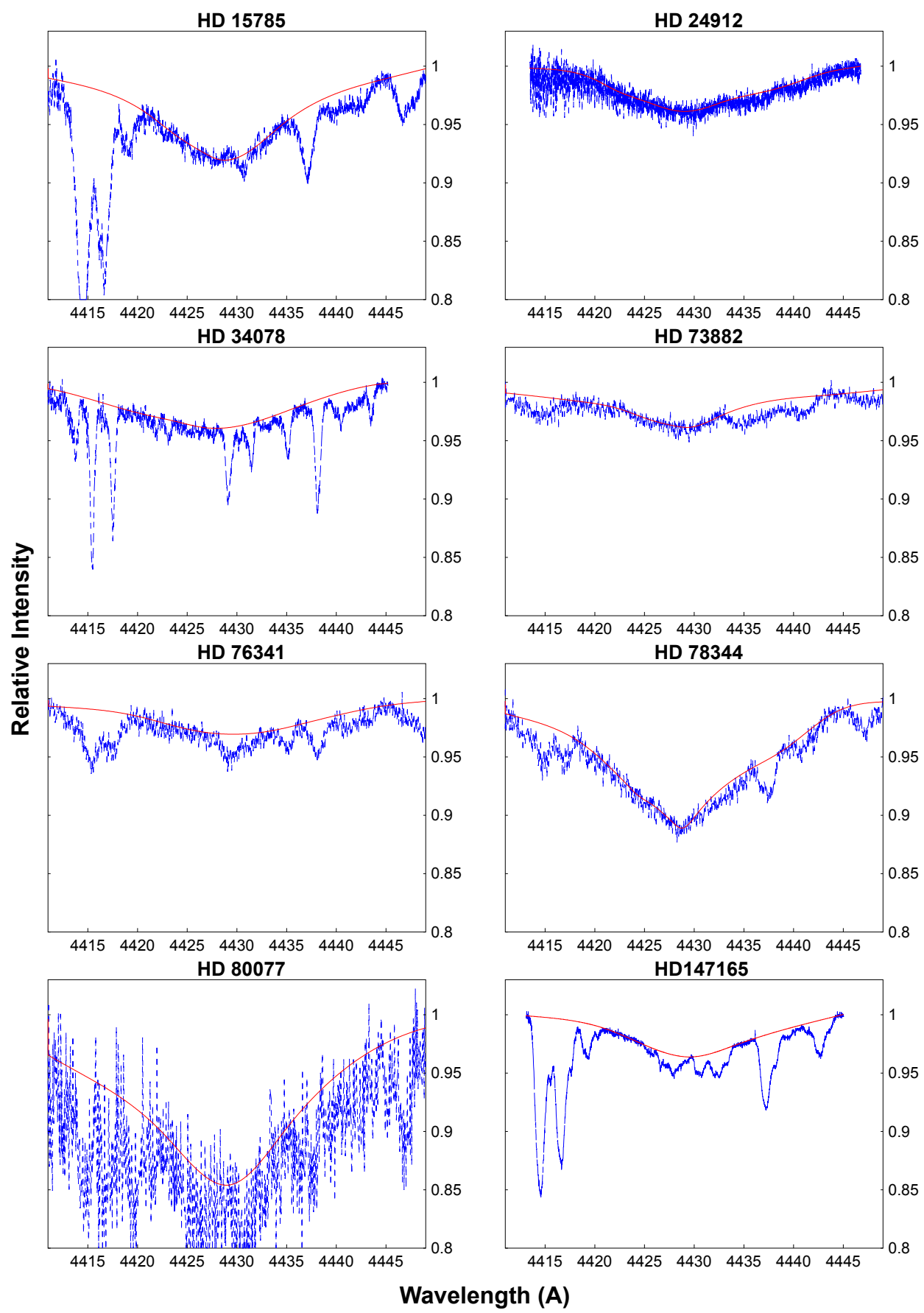
Tuairisg, S. Ó., Cami, J., Foing, B. H., et al. 2000, A&AS, 142, 225

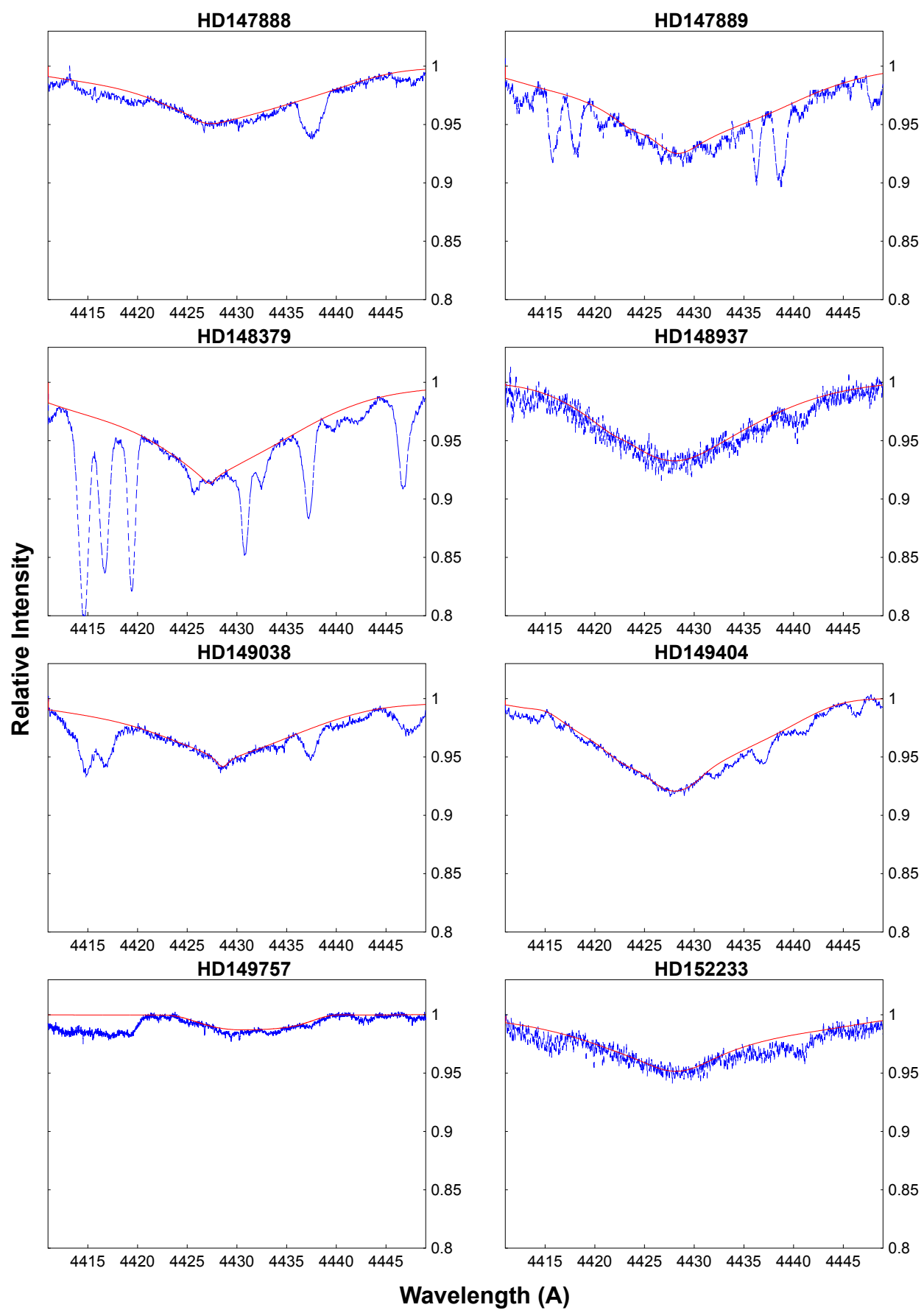
Vollmann, K., Eversberg, T., 2006, Astron. Nachr., 327, 862

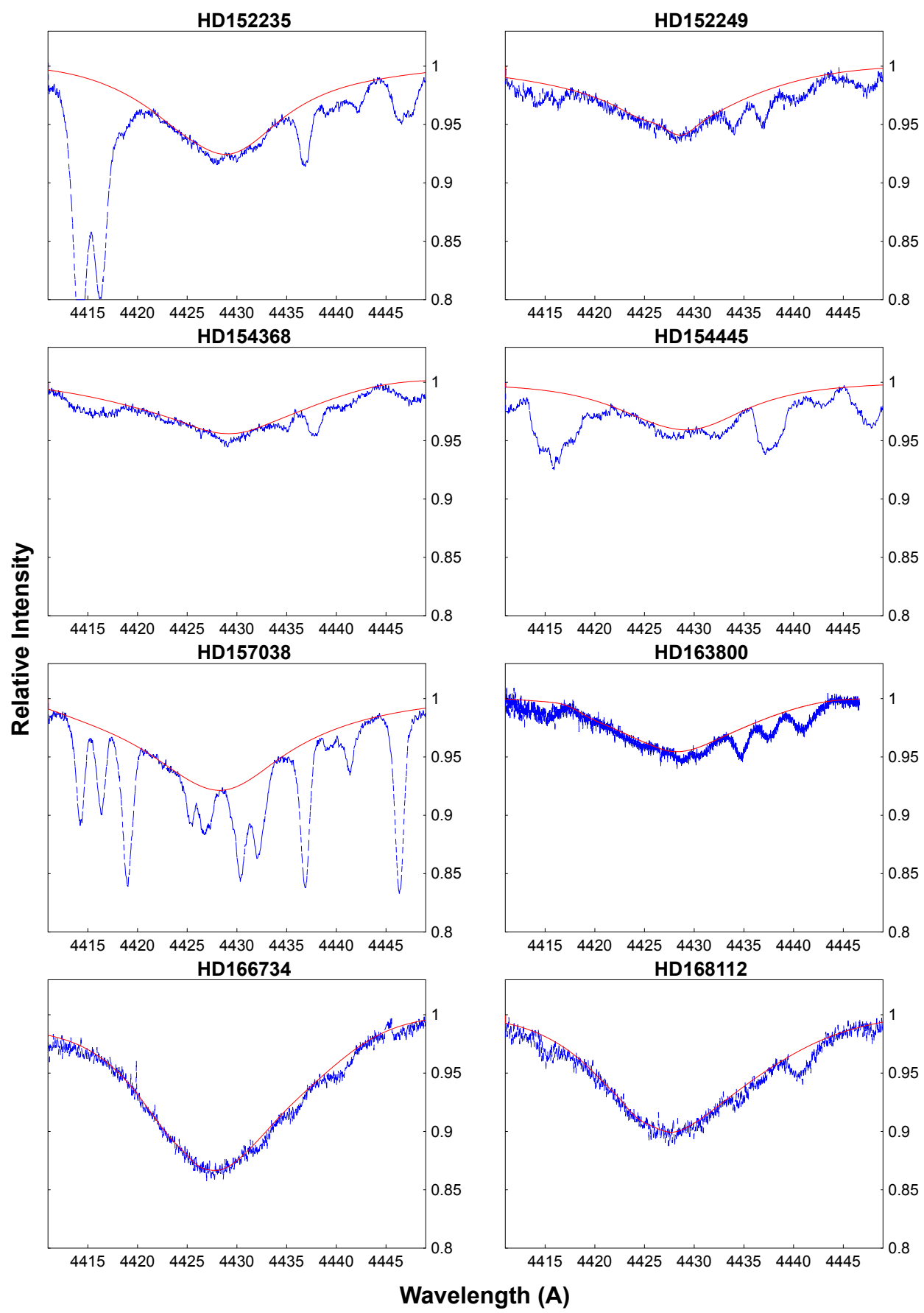
A. Appendix

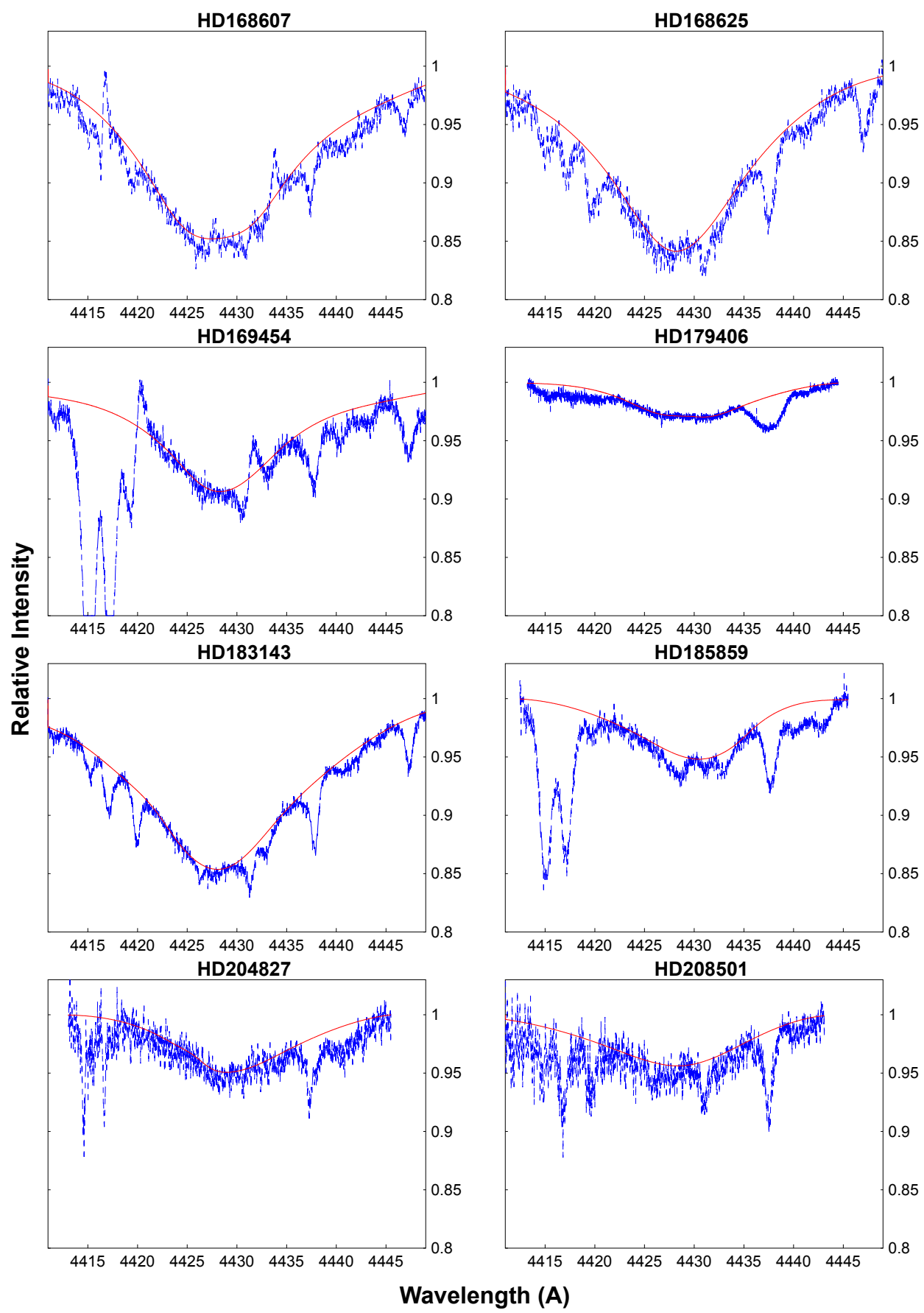
A.1. Profiles of 4430 DIB

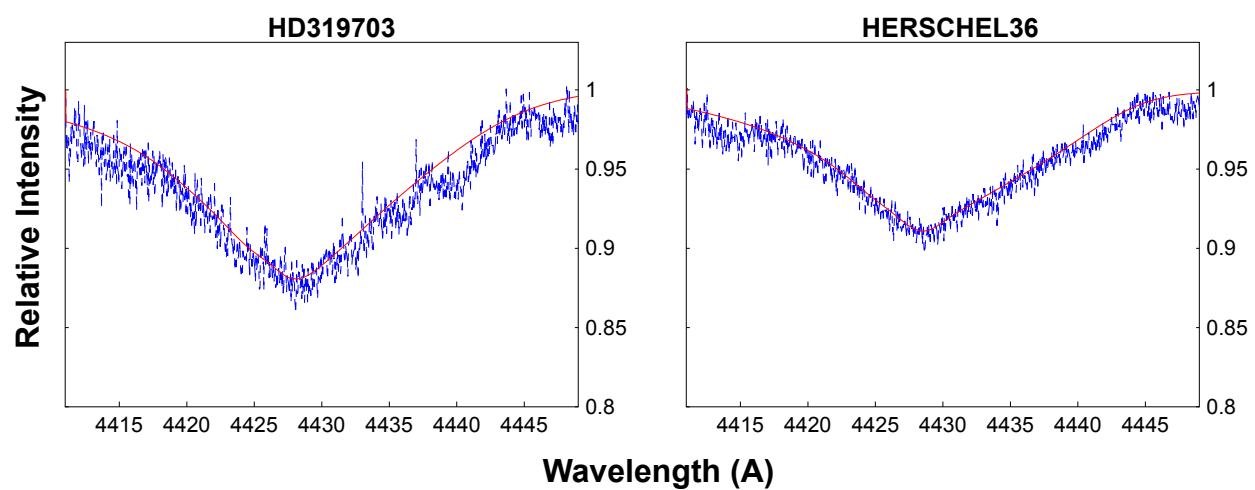




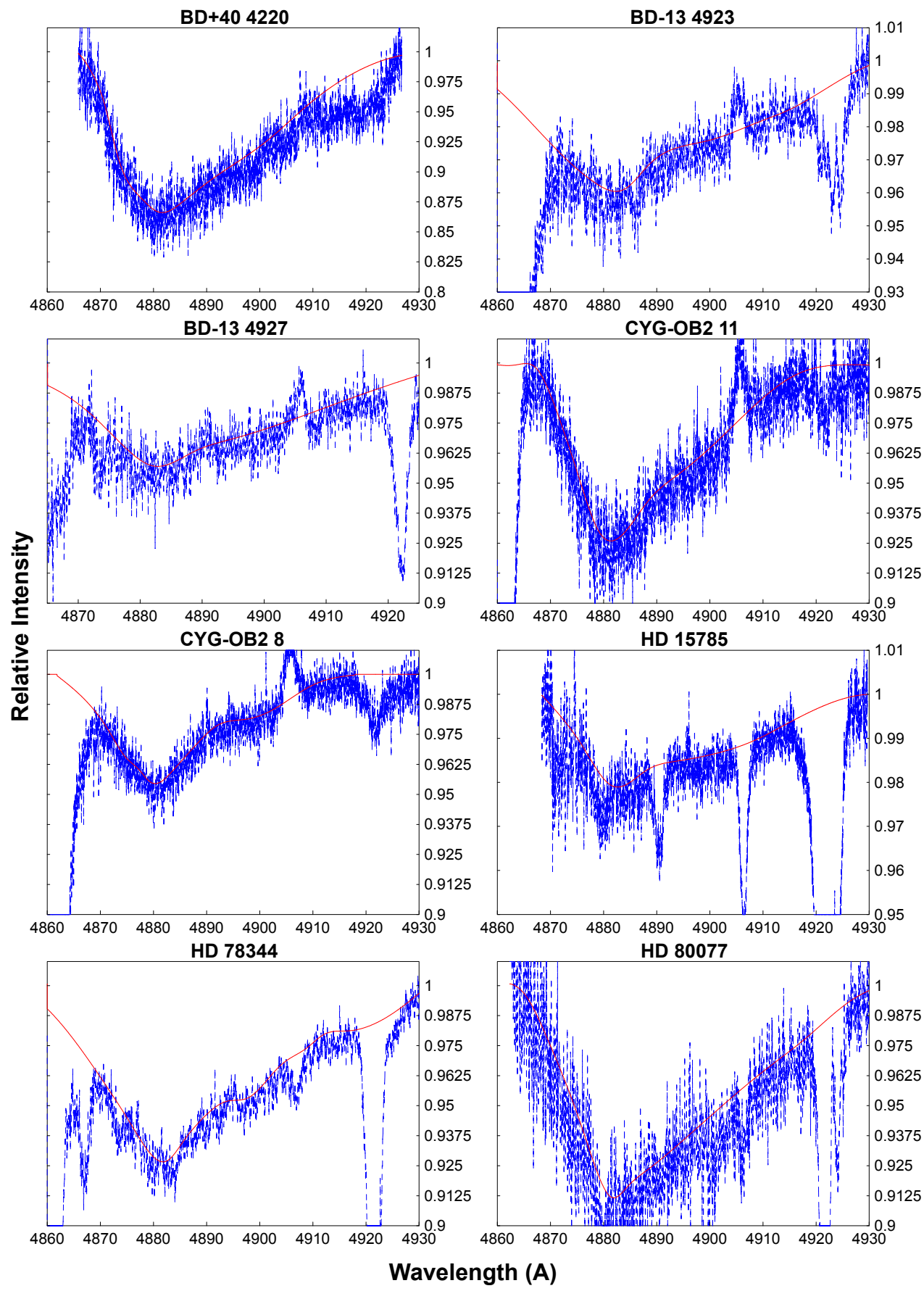


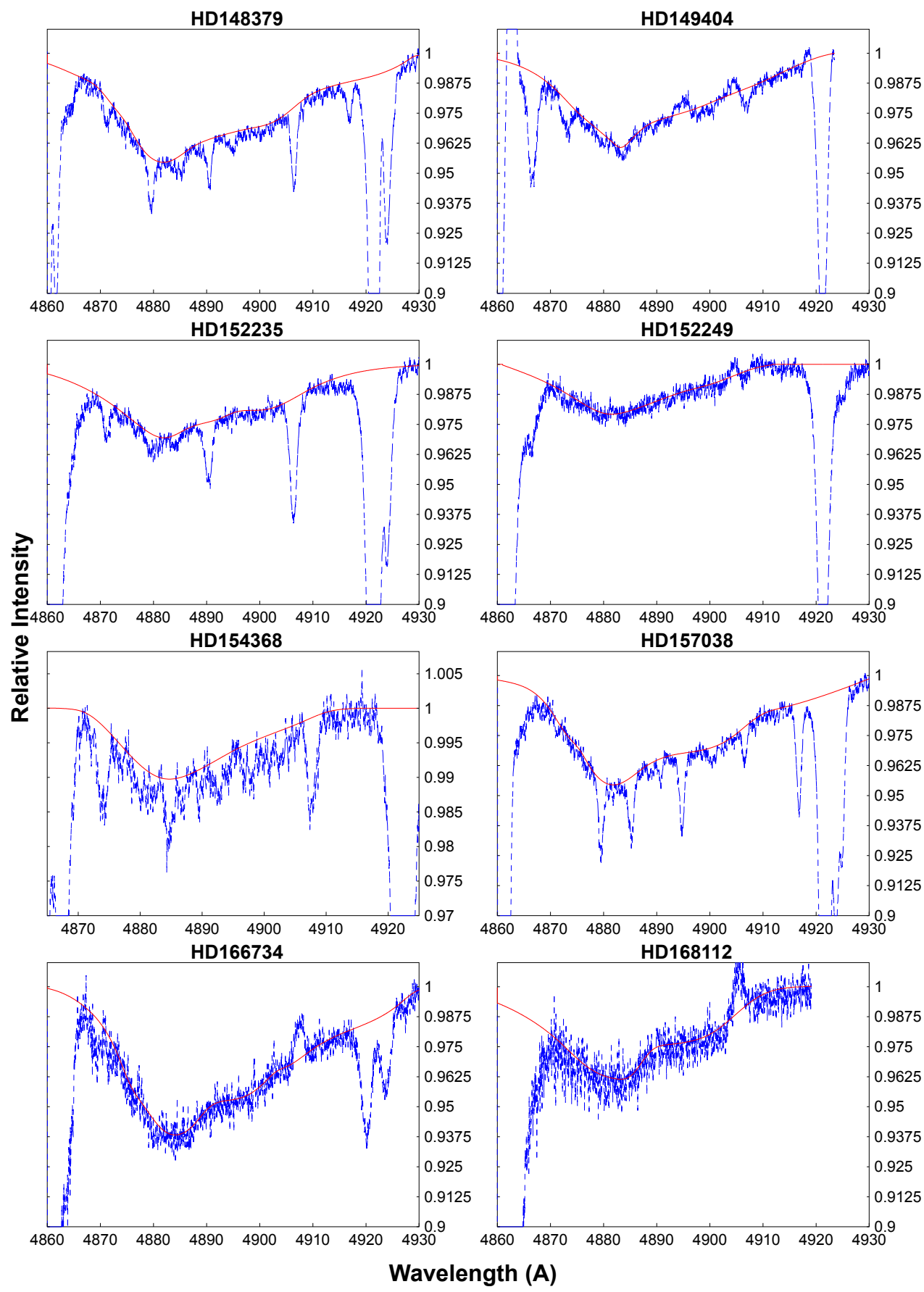


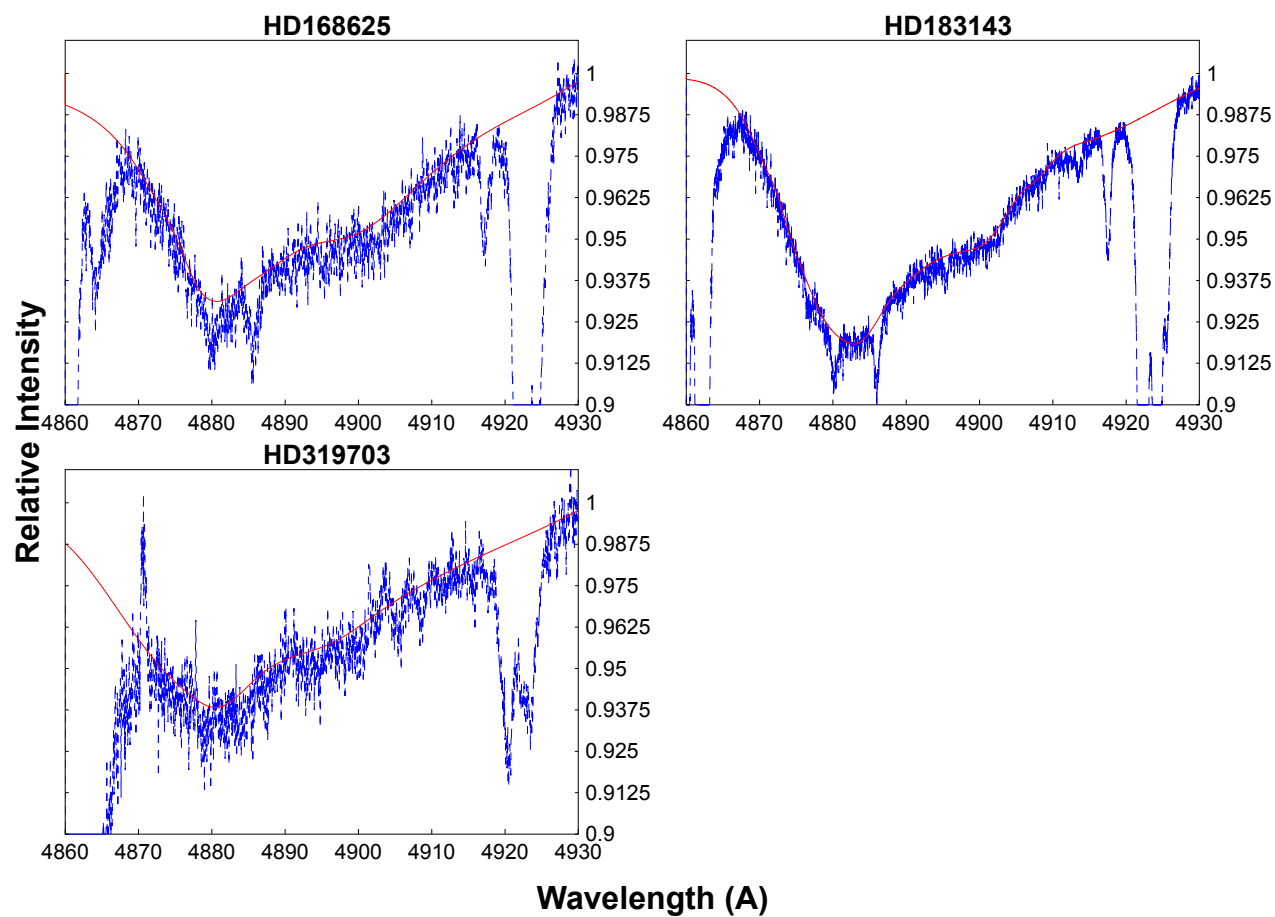




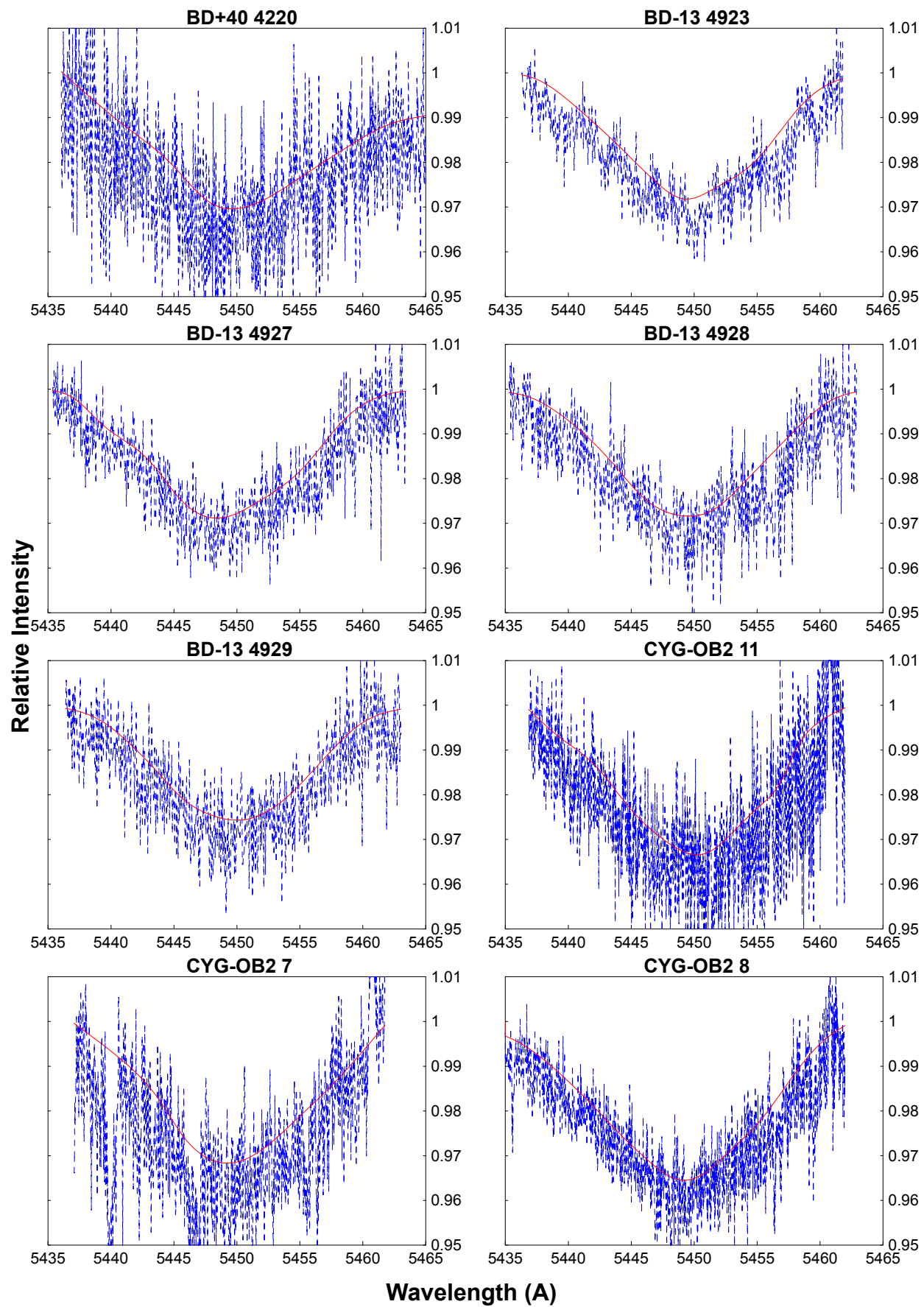
A.2. Profiles of 4882 DIB

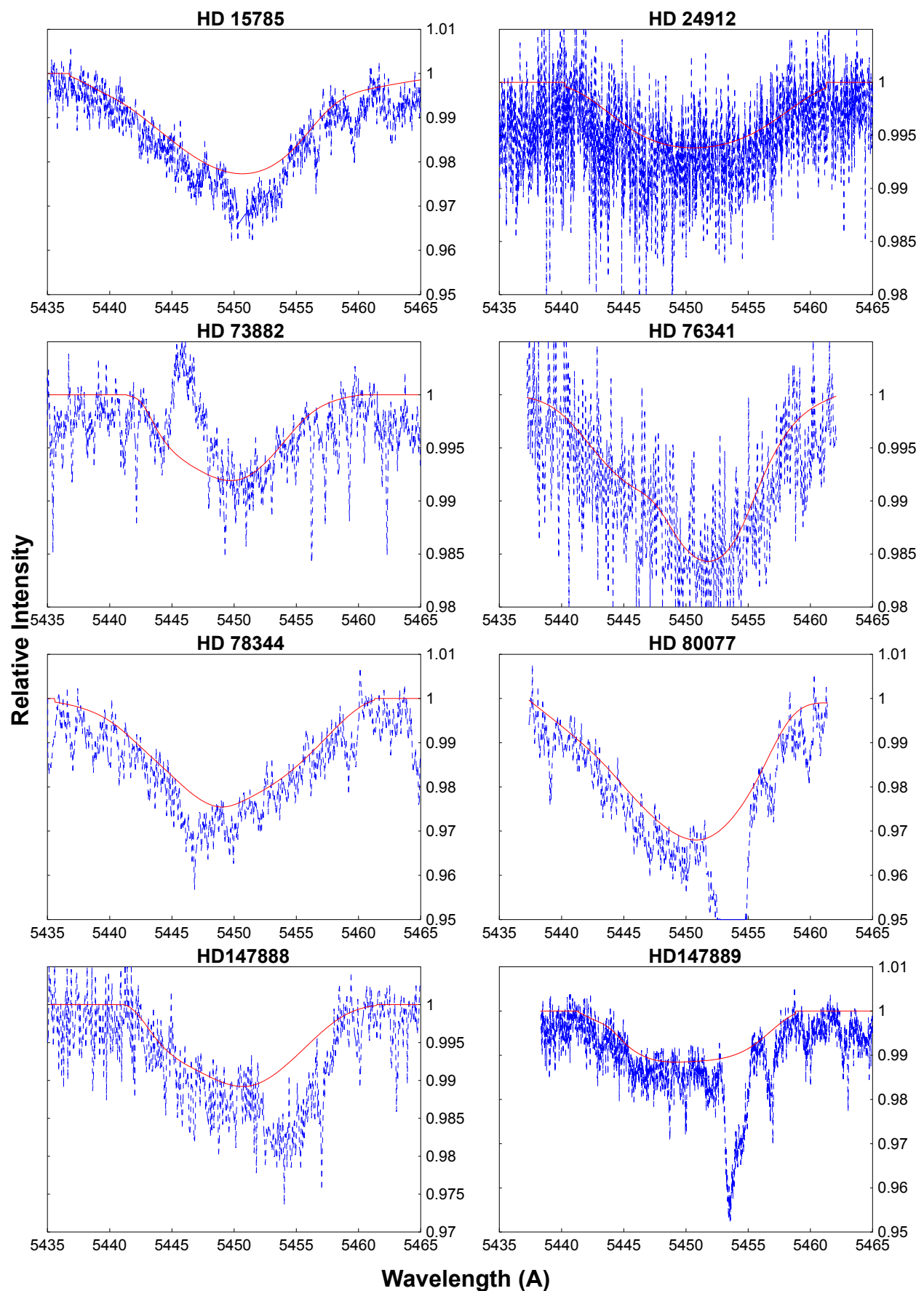


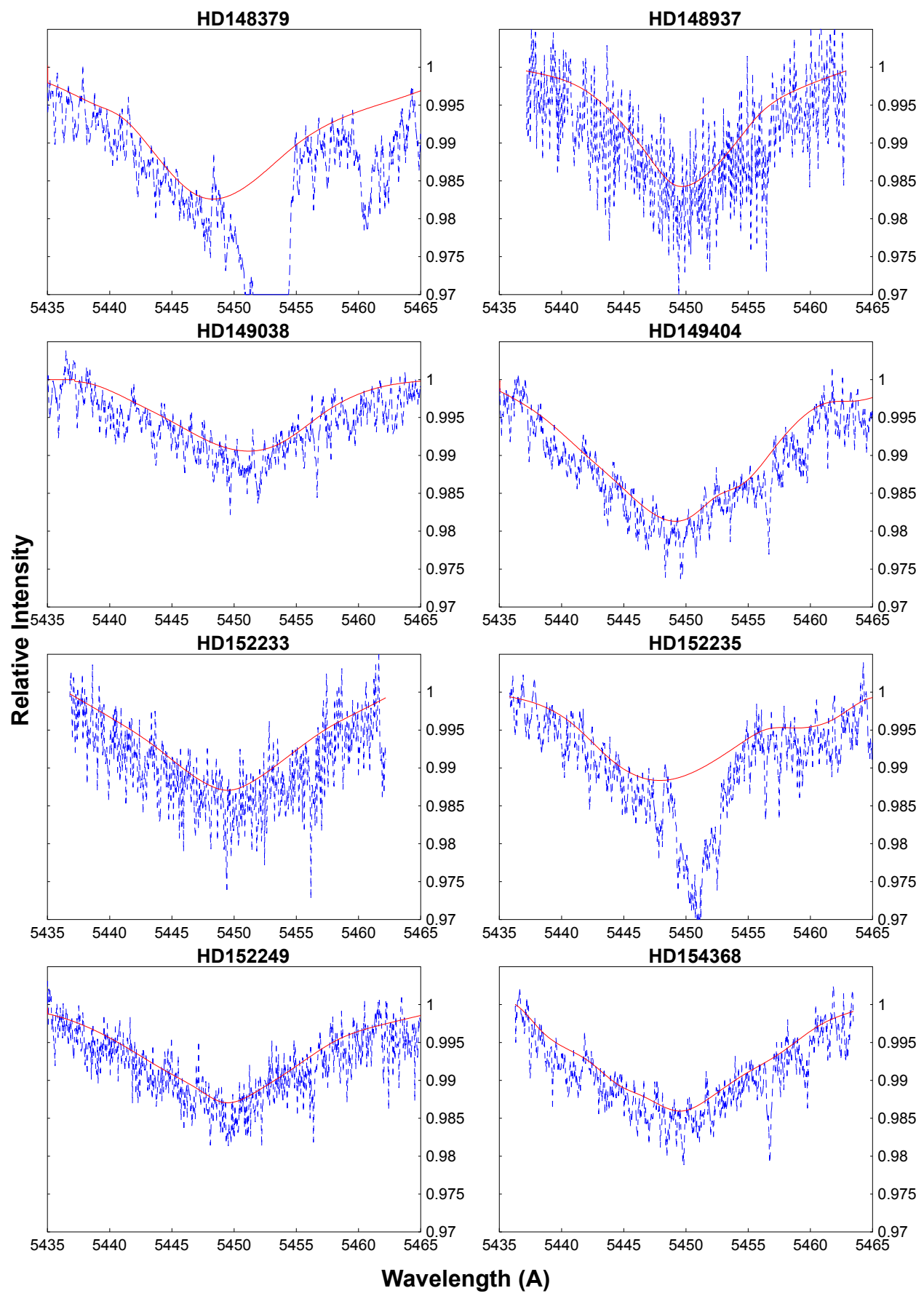


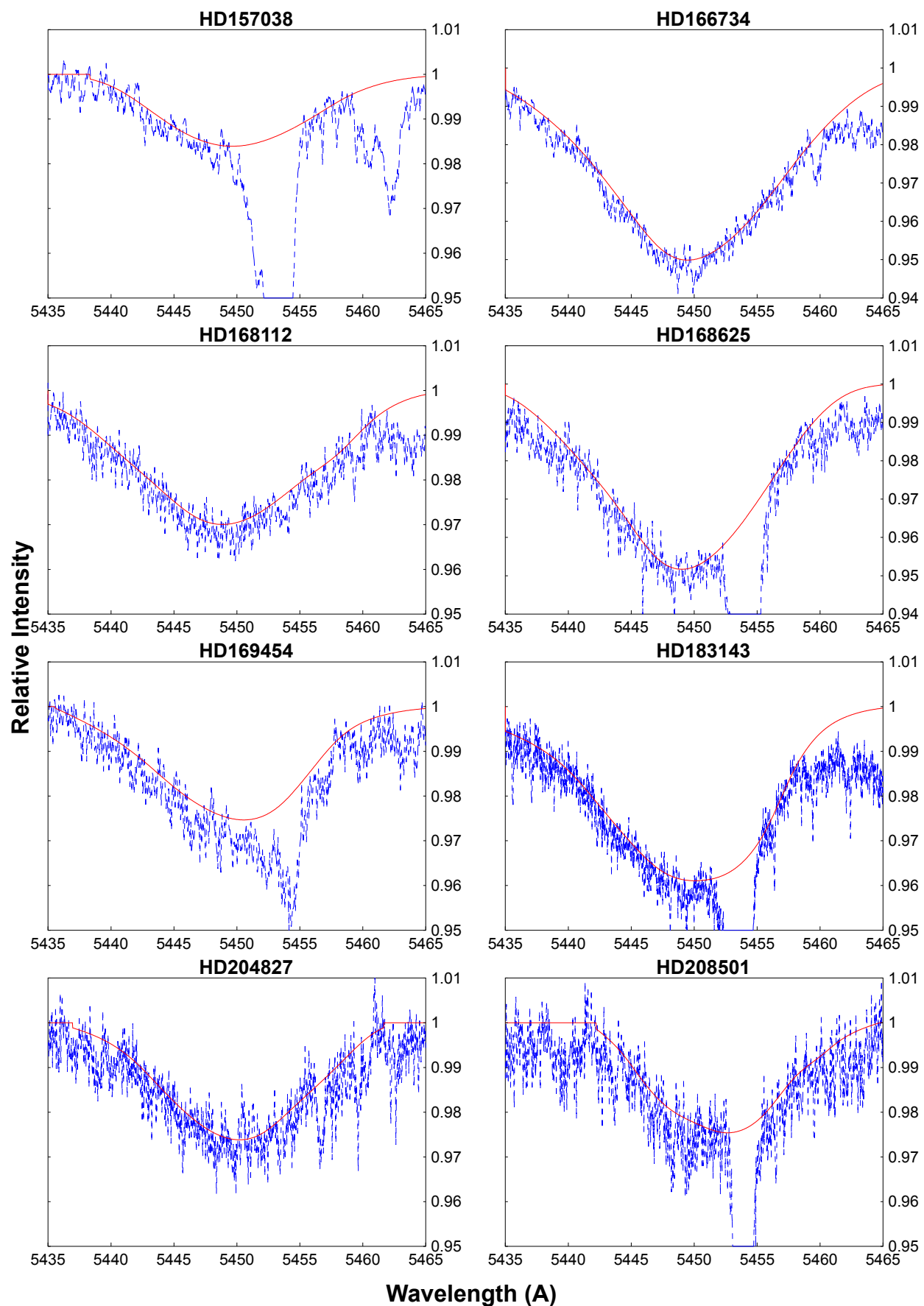


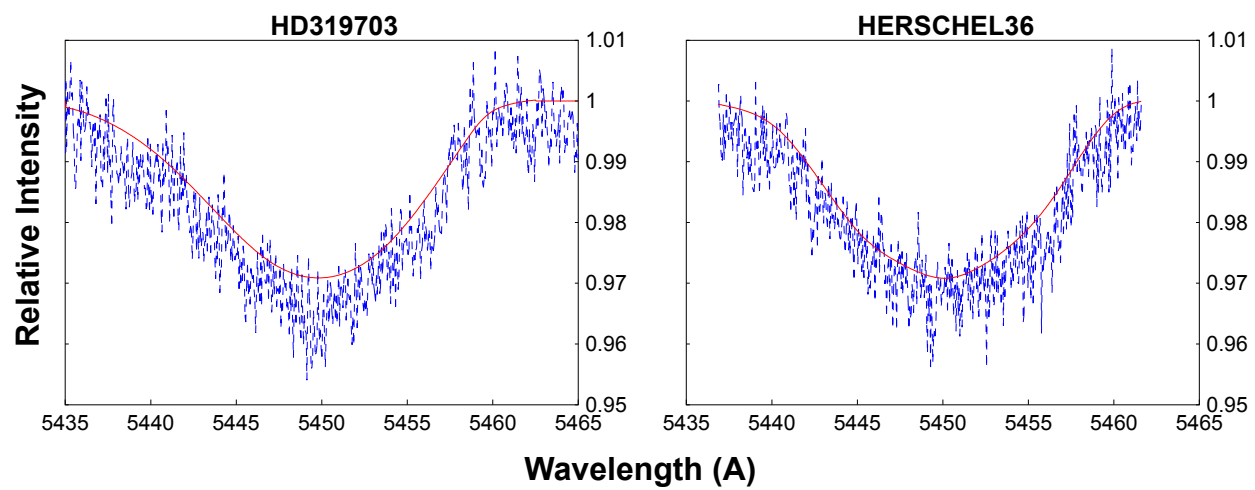
A.3. Profiles of 5450 DIB



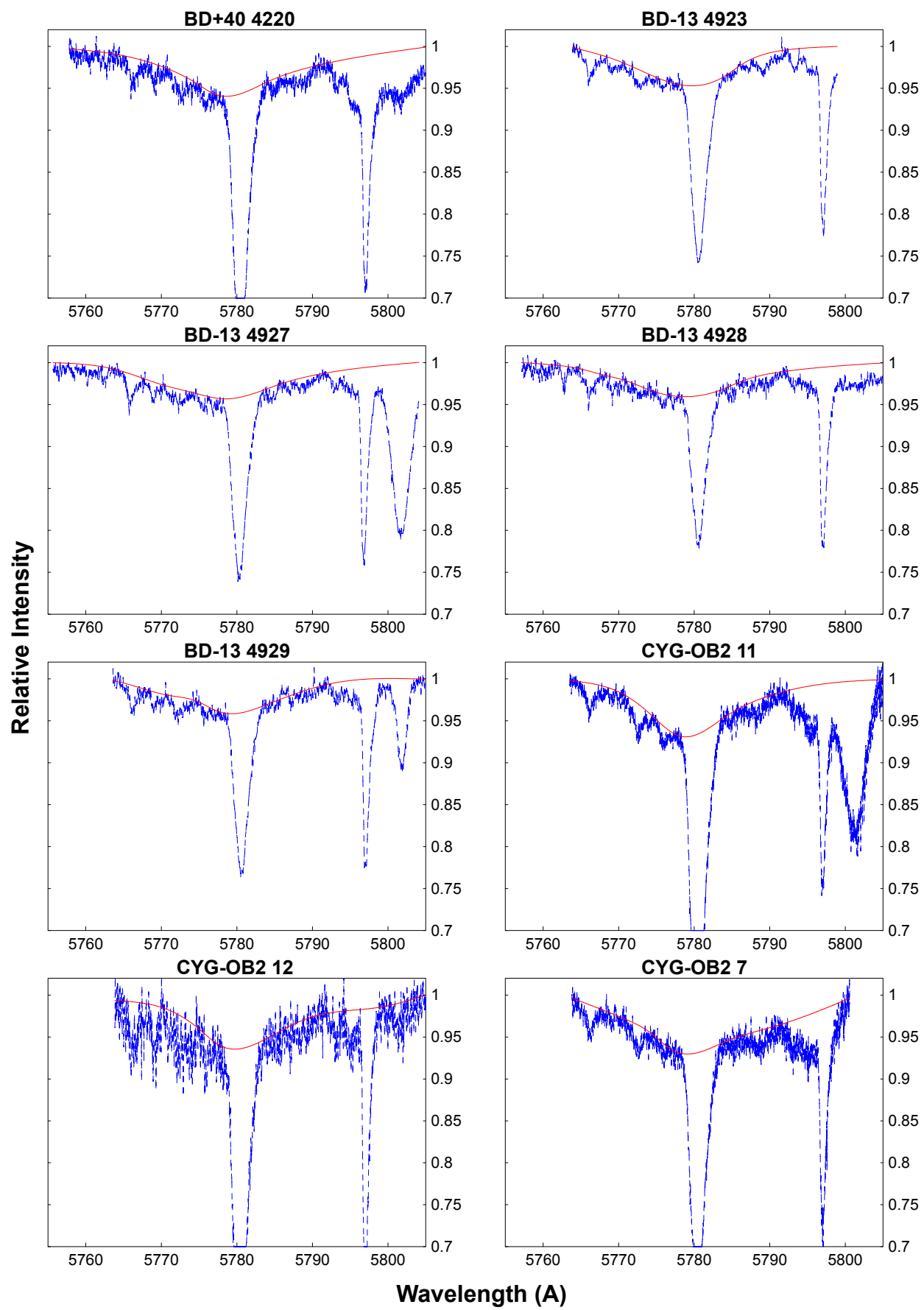


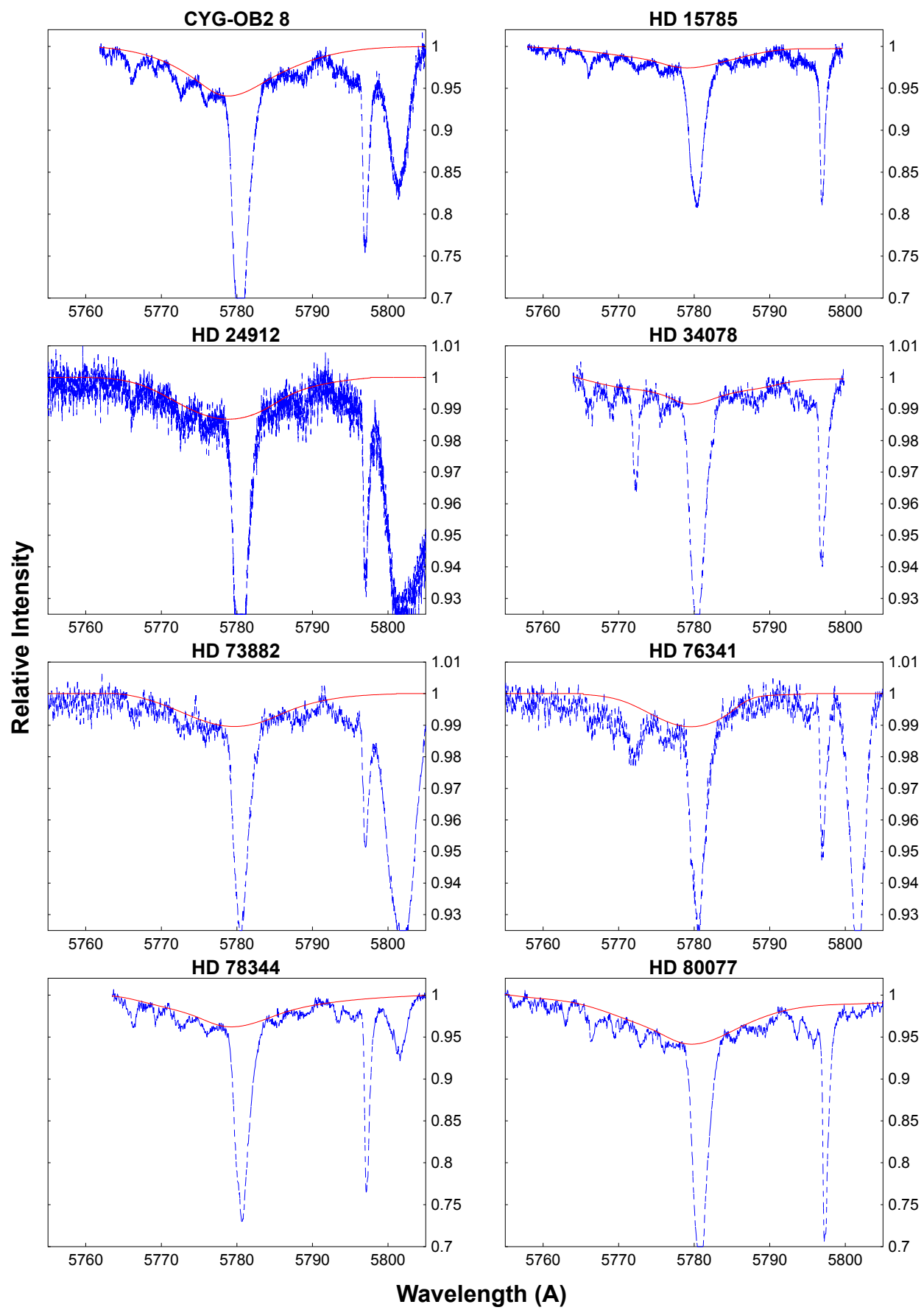


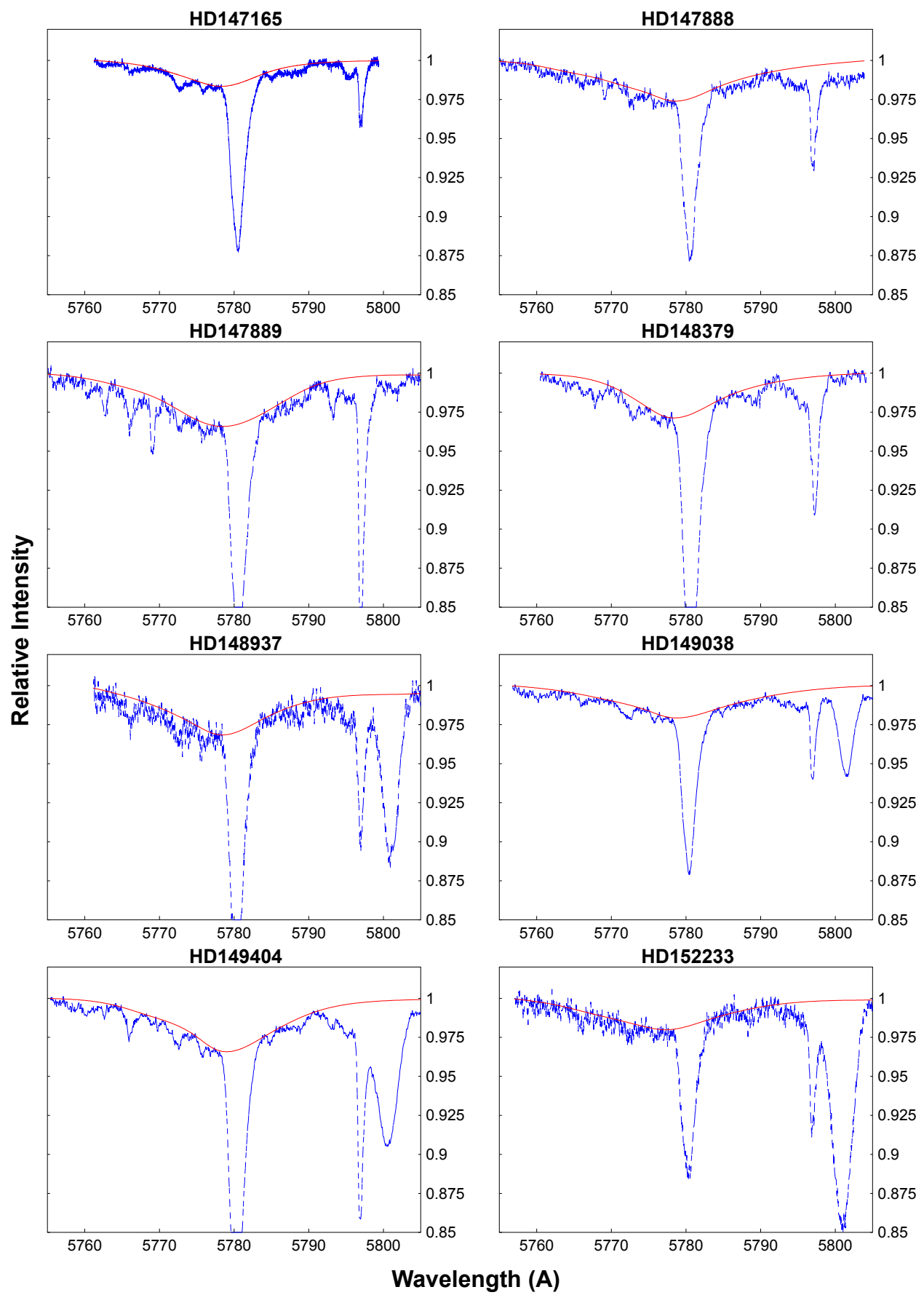


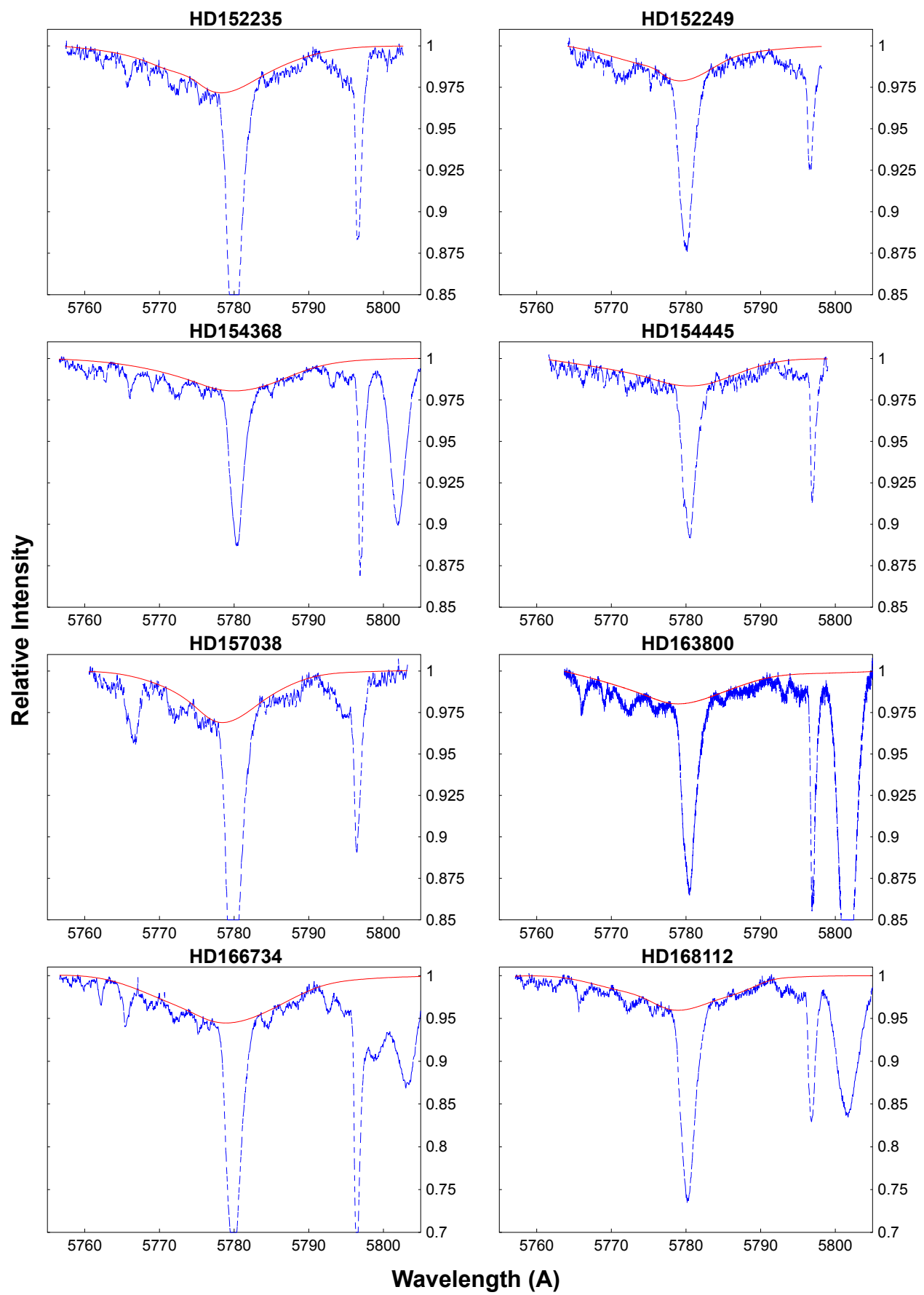


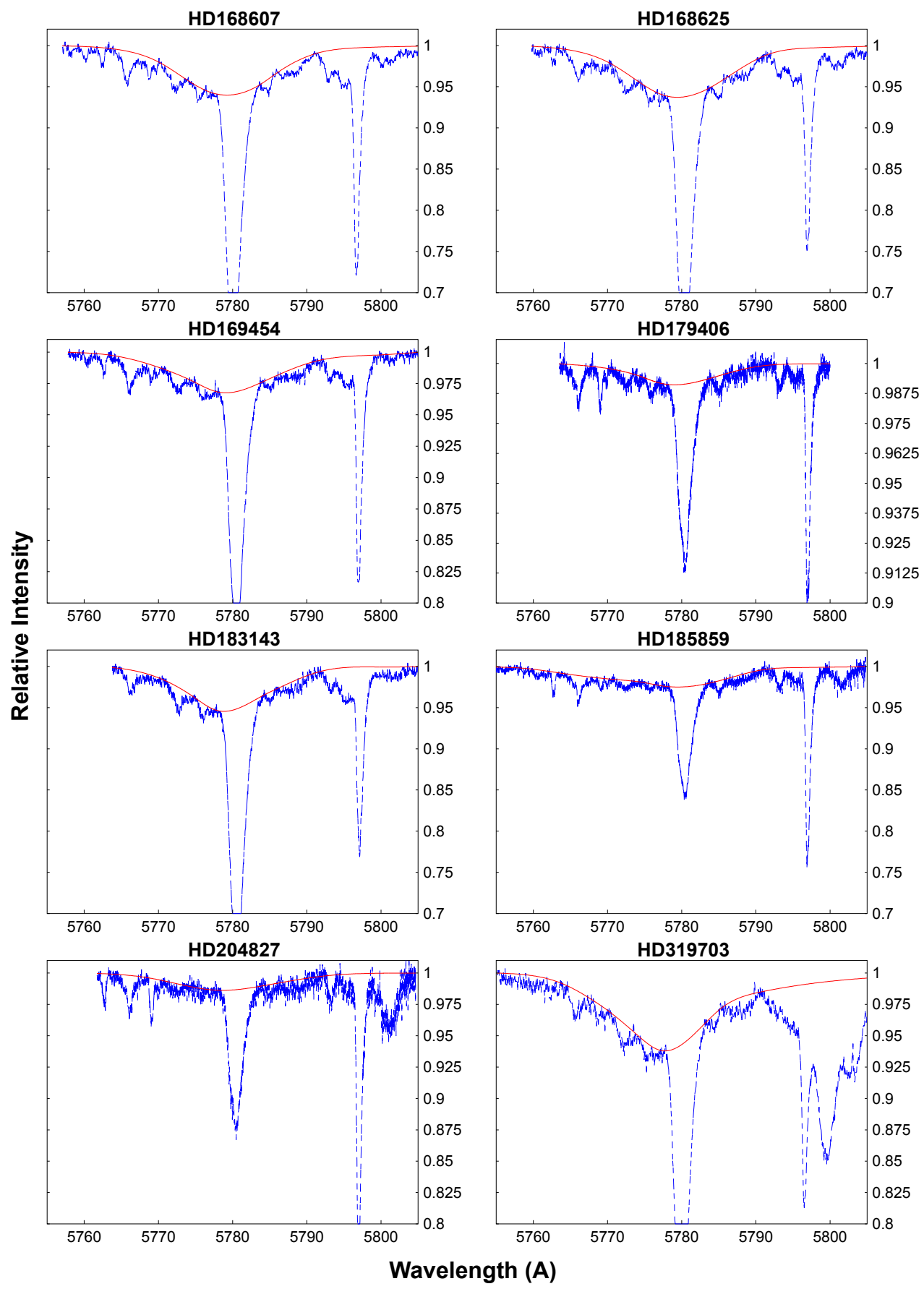
A.4. Profiles of 5779 DIB

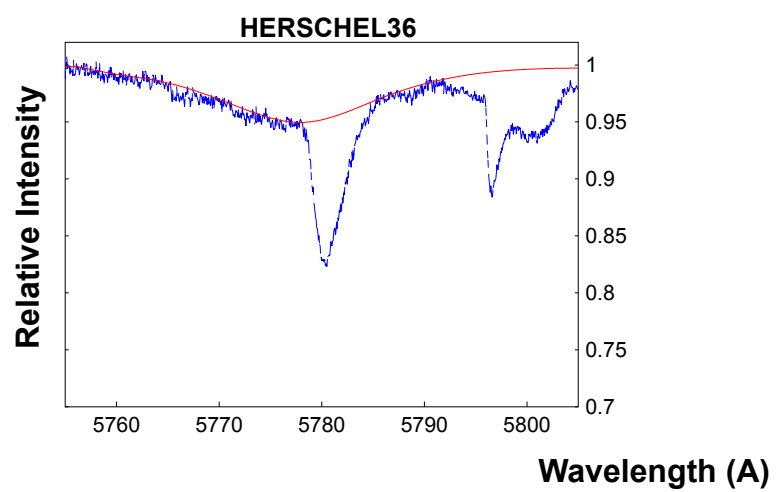












A.5. Profiles of 6175 DIB

